Ryo Suzuki, Yusuke Oda, Naoki Utoguchi, Kazuo Maruyama	Progress in the development of ultrasound-mediated gene delivery systems utilizing nano- and microbubbles	J. Controlled Release	149	36-41	2011
T. Kawazu, Y. Oda, K. Maruyama, et al.	Ultrasound-mediated Transfection with Liposomal Bubbles Delivers Plasmid DNA Directly into Nucleus.	Chemistry Letters	40	298-299	2011
Y. Ikeda-Dantsuji, R. Suzuki, K. Maruyama, et al.	Synergistic effect of ultrasound and antibiotics against Chlamydia trachomatis-infected human epithelial cells in vitro.	Ultrasonics Sonochem	18	425-430	2011

別紙4

<center>研究成果の刊行に関する一覧表</center>

雑誌

発表者氏名	論文タイトル名	発表誌名	巻号	ページ	出版年
R Plummer, Y Matsumura, et al.	A phase I clinical study of cisplatin-incorporated polymeric micelles (NC-6004) in patients with solid tumors.	Brit J Cancer	104	593-598	2011
M. Yasunaga, S. Manabe, Y. Matsumura	New Concept of Cytotoxic Immunoconjugate Therapy Targeting Cancer-Induced Fibrin Clots	Cancer Science	102 (7)	1396-1402	2011
M. Yasunaga, S. Manabe, Y. Matsumura	Cancer-stroma Targeting Therapy by Cytotoxic Immunoconjugate Bound to the Collagen 4 Network in the Tumor Tissue	Bioconjugate Chem	22(9)	1776-1783.	2011
K Kato, Y.Matsumura, et al.	Phase II study of NK 105, a paclitaxel-incorporating micellar nanoparticle, for previously treated advanced or recurrent gastric cancer.	Invest New Drugs,		published online.	2011
Y Matsumura.	Cancer stromal trageting (CAST) therapy.	Adv Drug Deliv Rev.	64	710-719	2012
Y Saito, M Yasunaga, Y Matsumura, et al.	The inhibition of pancreatic cancer invasion-metastasis cascade in both cellular signal and blood coagulation cascade of tissue factor by it	Eur J Cancer.	47	2230-2239	2011
M Rafi, N Nishiyama, et al.	Polymeric micelles incorporating (1,2-diaminocyclohexane) platinum (II) suppress the	J. Controlled Release		In press	2012

H Cabral, N Nishiyama, et al.	Accumulation of sub-100 nm polymeric micelles in poorly permeable tumours depends on size.	Nature Nanotech.	6(12)	815-823	2011
Ryo Suzuki, Yusuke Oda, Naoki Utoguchi, Kazuo Maruyama	Progress in the development of ultrasound-mediated gene delivery systems utilizing nano- and microbubbles	J. Controlled Release	149	36-41	2011
T. Kawazu, Y. Oda, K. Maruyama, et al.	Ultrasound-mediated Transfection with Liposomal Bubbles Delivers Plasmid DNA Directly into Nucleus.	Chemistry Letters	40	298-299	2011
Y. Ikeda-Dantsuji, R. Suzuki, K. Maruyama, et al.	Synergistic effect of ultrasound and antibiotics against Chlamydia trachomatis-infected human epithelial cells in vitro.	Ultrasonics Sonochem	18	425-430	2011

Full Paper

A Phase I clinical study of cisplatin-incorporated polymeric micelles (NC-6004) in patients with solid tumours

R Plummer[1], RH Wilson[2], H Calvert[1,7], AV Boddy[1], M Griffin[1], J Sludden[1], MJ Tilby[1], M Eatock[2], DG Pearson[3], CJ Ottley[3], Y Matsumura[4], K Kataoka[5] and T Nishiya*[,6]

[1]Northern Institute for Cancer Research, Paul O'Gorman Building, Framlington Place, Newcastle upon Tyne NE2 4AD, UK; [2]Centre for Cancer Research and Cell Biology, Queen's University Belfast, Lisburn Road, Belfast BT9 7AB, Northern Ireland, UK; [3]Department of Earth Sciences, University of Durham, Science Labs, Durham DH1 3LE, UK; [4]Investigative Treatment Division, Research Center for Innovative Oncology, National Cancer Center Hospital East, 6-5-1 Kashiwanoha, Kashiwa, Chiba 277-8577, Japan; [5]Department of Materials Engineering, Graduate School of Engineering, and Center for Disease Biology and Integrative Medicine, Graduate School of Medicine, The University of Tokyo, 7-3-1 Hongo, Bunkyo-ku, Tokyo 113-8656, Japan; [6]Division of Clinical Study, NanoCarrier Co. Ltd, Yaesu Yamagata Building, 3-2-2 Nihonbashi, Chuo-ku, Tokyo 103-0027, Japan

BACKGROUND: On the basis of preclinical studies of NC-6004, a cisplatin-incorporated micellar formulation, we hypothesised that NC-6004 could show lower toxicity than cisplatin and show greater anti-tumour activity in phase I study.

METHODS: A total of 17 patients were recruited in a range of advanced solid tumour types. NC-6004 was administered intravenously (i.v.) every 3 weeks. The dose escalation started at $10\,mg\,m^{-2}$ and was increased up to $120\,mg\,m^{-2}$ according to the accelerated titration method and modified Fibonacci method.

RESULTS: One dose-limiting toxicity (DLT) occurred in a patient who was given $90\,mg\,m^{-2}$ of NC-6004, otherwise any significant cisplatin-related toxicity was not observed or generally mild toxicity was observed. Despite the implementation of post-hydration and pre-medication regimen, renal impairment and hypersensitivity reactions still developed at $120\,mg\,m^{-2}$, which led to the conclusion that the maximum tolerated dose was $120\,mg\,m^{-2}$, and the recommended dose was $90\,mg\,m^{-2}$, although DLT was not defined as per protocol. Stable disease was observed in seven patients. The maximum concentration and area under the concentration–time curve of ultrafilterable platinum at $120\,mg\,m^{-2}$ NC-6004 were 34-fold smaller and 8.5-fold larger, respectively, than those for cisplatin.

CONCLUSION: The delayed and sustained release of cisplatin after i.v. administration contributes to the low toxicity of NC-6004.
British Journal of Cancer advance online publication, 1 February 2011; doi:10.1038/bjc.2011.6 www.bjcancer.com
© 2011 Cancer Research UK

Keywords: cisplatin; DDS; EPR effect; NC-6004; phase I study; polymer micelle

Cisplatin, cis-diamminedichloroplatinum (II), is a platinum (Pt)-based chemotherapy drug used to treat various types of cancers. Clinical use of cisplatin is, however, associated with irreversible renal toxicity, which necessitates the use of pre- and post-hydration regimens, and excludes its use in patients with less than normal renal function (Pinzani et al, 1994). Cisplatin therapy also causes neurotoxicity, gastrointestinal toxicity (nausea and vomiting), haematological toxicity, and irreversible ototoxicity (Hartmann and Lipp, 2003). Furthermore, its anti-tumour efficacy continues to be limited by either intrinsic or acquired resistance (Kartalou and Essigmann, 2001). To overcome these cisplatin-related disadvantages, various types of Pt analogues, including carboplatin, oxaliplatin, satraplatin, and picoplatin have been developed (Kelland and Sharp, 1999; Judson and Kelland, 2000; Sharp et al, 2002). Another potential method for improving the therapeutic indices of cisplatin is the incorporation of cisplatin into polymeric micelles of varying size in the range of 20–100 nm composed of polyethylene glycol (PEG)-poly (amino acid) block co-polymers, in which PEG constitutes the hydrophilic outer shell of the micelle and cisplatin is incorporated into hydrophobic inner core of the micelle (Yokoyama et al, 1996; Nishiyama et al, 1999, 2001b, 2003; Nishiyama and Kataoka, 2001a).

Preclinical studies carried out on NC-6004, cisplatin-incorporated polymeric micelles composed of PEG-poly (glutamic acid) block co-polymers via polymer–metal complex formation (Figures 1 and 2), have indicated that it is preferentially distributed to tumours by enhanced permeability and retention effect (Matsumura and Maeda, 1986; Maeda and Matsumura, 1989; Maeda et al, 2000; Maeda, 2001), and demonstrates significantly lower toxicity than cisplatin and greater anti-tumour activity (Uchino et al, 2005). On the basis of these results, a phase I clinical trial of NC-6004 in patients with advanced solid tumours has been carried out. The objectives of the study were to determine the maximum-tolerated dose (MTD), the recommended dose (RD) for the phase II, the dose-limiting toxicities (DLTs), the safety and tolerability profile, and to explore evidence of anti-tumour activity, and the pharmacokinetics of NC-6004.

*Correspondence: Dr T Nishiya;
E-mail address: nishiya@nanocarrier.co.jp
[7] Current address: UCL Cancer Institute, Paul O'Gorman Building, 72 Huntley Street, London WC1E 6BT, UK.

$CH_3O\text{-}(CH_2CH_2O)_n\text{-}CH_2CH_2CH_2\text{-}NH\text{-}(CO\text{-}CH\text{-}NH)_{m\text{-}x}\text{-}(CO\text{-}CH\text{-}NH)_x\text{-}H$
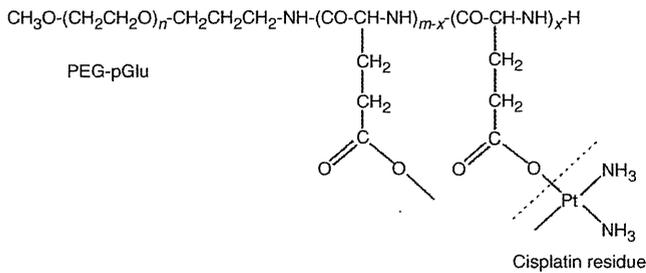
PEG-pGlu

Cisplatin residue

Figure 1 Structure of cisplatin-PEG-poly(glutamic acid) block co-polymer conjugate. PEG-pGlu, PEG-poly(glutamic acid); n, approximately 268; m, approximately 40; x, approximately 24.
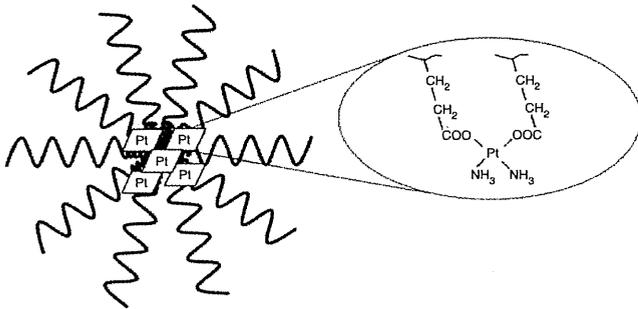

Figure 2 Structure of cisplatin-incorporated polymeric micelle, NC-6004. Core part, cisplatin residue bound to poly-L-glutamic acid. Exterior part, PEG.

PATIENTS AND METHODS

Ethics

The trial was an open-label, dose-escalating, phase I study conducted at two sites in the United Kingdom; Newcastle General Hospital and Belfast City Hospital. All procedures were reviewed by Independent Ethics Committees, and were in accordance with the protocol, the Helsinki Declaration (October 2000, and clarified 2002 and 2004), the Note for Guidance on Good Clinical Practice (CPMP/ICH/135/95) approved in July 1996, and the applicable regulatory requirements.

Administration of therapeutic agent

NC-6004 (NanoCarrier Co., Ltd Chiba, Japan) was a sterile solution containing the equivalent of $2.5 \, mg \, ml^{-1}$ cisplatin and could be diluted in 5% dextrose before administration.

Dosing was performed by intravenous (i.v.) infusion of 500 ml over 60 min, once every 3 weeks. Following the observation of renal toxicities, hydration using 1000 to 1500 ml of fluid, immediately after NC-6004 infusion, was implemented for the rest of the study. Later in the study, after the occurrence of four events of hypersensitivity reactions, the following prophylactic treatment was implemented at each cycle for all patients; 30 min before infusion – dexamethasone 20 mg i.v., chlorphenamine 10 mg i.v., and ranitidine 50 mg i.v. Oral dexamethasone 4 mg (twice a day), ranitidine 150 mg (twice a day), and chlorphenamine 4 mg (three times a day) could also be given if necessary on a per-patient individualised basis for 48 h after infusion.

Patients' eligibility and dose escalation

Patients with histologically confirmed advanced solid tumours, for which no standard therapy exists or has failed therapy, were eligible for enrolment in this study, provided that the following criteria were met: Eastern Cooperative Oncology Group performance

Table 1 Dose modification for changes in estimated creatinine clearance or ^{51}Cr-EDTA clearance

Estimated creatinine clearance/GFR	NC-6004 dose	^{51}Cr-EDTA clearance (in ml min^{-1})	NC-6004 dose
$>60 \, ml \, min^{-1}$	100% of dose	>60	100% of dose
$50\text{-}60 \, ml \, min^{-1}$	80% of dose	$40\text{-}60$	50% of dose
$<50 \, ml \, min^{-1}$ or any drop from baseline by $>10\%$ calculated GFR	^{51}Cr-EDTA clearance measurement	<40	Discontinue

Abbreviations: ^{51}Cr-EDTA clearance = chromium-51-ethylenediaminetetraacetic acid clearance; GFR = glomerular filtration rate.

status of $\leqslant 2$; age of $\geqslant 18$ years; life expectancy of at least 12 weeks; a normal haematological profile, renal function, hepatic function, and serum calcium level, no more than one previous course of Pt therapy, with maximum cumulative doses of $480 \, mg \, m^{-2}$ of cisplatin, $1040 \, mg \, m^{-2}$ of oxaliplatin, or $42 \, mg \, ml^{-1} \, min^{-1}$ (min = minutes) cumulative area under the concentration-time curve (AUC) of carboplatin, and no chemotherapy, no radiotherapy (except palliative radiation delivered to $<20\%$ of bone marrow), no immunotherapy, or no corticosteroids (greater than 10 mg per day of prednisone or equivalent) within 4 weeks before entering the study or patients who have not recovered from adverse events because of agents administered more than 4 weeks earlier. Patients who had severe hypersensitivity to Pt compounds, ototoxicity assessed by audiometry (except senile hearing loss at high frequency) or other neurotoxicity $\geqslant$ grade 2 were ineligible for enrolment in the study. Patients were excluded if they were pregnant or lactating.

The dose of NC-6004 is, hereafter, always expressed as cisplatin equivalent $mg \, m^{-2}$ of body surface area per injection. The starting dose of NC-6004 was $10 \, mg \, m^{-2}$, one-tenth of the lethal dose in 10% in rat or one-third of the toxic dose low in dog. In stage 1, (accelerated titration method), each dose was escalated at twice the previous dose level until drug-related toxicity $\geqslant$grade 2 was seen in cycle 1. Once the first drug-related toxicity $\geqslant$grade 2 in cycle 1 was seen, a minimum cohort of three patients was recruited, and each dose was defined as 150% of the previous one in stage 2 (modified Fibonacci method) until MTD was reached. The dose was modified according to the estimated creatinine clearance (Cl)/GFR measured before each administration of NC-6004 as detailed in Table 1. Intra-patient dose escalation was not permitted.

Toxicity was graded by the Common Terminology Criteria for Adverse Events version 3.0. MTD was defined as the dose at which one-third of patients experience DLT, and RD was the highest dose, which gave rise to no more than one DLT out of a cohort of six patients. DLTs were defined as grade 4 neutropenia associated with fever ($\geqslant 38.5°C$) or diarrhoea $\geqslant$ grade 2, grade 4 neutropenia lasting $\geqslant 5$ days without fever, grade 4 thrombocytopenia for $\geqslant 5$ days, grade 3 or higher non-haematological toxicity (except liver transaminase elevation, or nausea or vomiting treatable by anti-emetic), and treatment delay >2 weeks before start of next cycle of treatment because of unresolved toxicity.

Pretreatment assessment and follow-up studies

Assessment of medical history was completed during the 21 days before the start of NC-6004 dosing. Safety was monitored throughout the trial until the end of trial visit. In the treatment phase, physical assessment, routine laboratory analysis, estimated creatinine Cl, and concurrent illness/therapy were reviewed on day 1 of cycle 1, then every week until week 7 and then every 3 weeks thereafter, and at withdrawal from the trial. Adverse events were reviewed during the first 4 days of cycle 1, then every week from

weeks 2 to 7 and then every 3 weeks from week 7 onwards, and at withdrawal. The CT/MRI scans of all target and non-target lesions were performed every 6 weeks and at withdrawal, and tumour markers, if applicable, were assessed every 3 weeks. The Response Evaluation Criteria in Solid Tumour (RECIST) was used to define lesions and the criteria for objective tumour response. For pharmacokinetic analysis, blood samples were taken at 0, 2, 4 and 8 h after administration on days 1, 2, 3, 4, 8, 15, and 22 and before cycle 2.

Pharmacokinetic analysis

Blood samples were centrifuged and separated plasma was processed to produce three different forms of sample: total plasma, gel filtrate and ultrafiltrate. Plasma (1 ml) was stored for total-plasma Pt analysis. Plasma (1 ml) was centrifuged with a molecular weight cutoff of 200 000 Da, and the eluant was analysed for micellar Pt. Finally, a further 1 ml of plasma was centrifuged with a molecular weight cutoff of 30 000 Da to give an ultrafiltrate for the determination of low-molecular weight Pt species, including cisplatin. Concentration of total plasma Pt and micellar Pt (gel filtrate) were measured using atomic absorption spectrometry on Analyst 600 (Perkin-Elmer, Waltham, MA, USA) against standards prepared in plasma. Ultrafiltrate samples were analysed by inductively coupled plasma mass spectrometry on Element 2 (Thermo Scientific Inc., Waltham, MA, USA) against centrifuged Pt standards at Durham University. Pharmacokinetic analysis was performed using WinNonlin version 1.3 (Pharsight Corporation, Mountain View, CA, USA) to calculate the maximum concentration (C_{max}), the time to the maximum concentration (T_{max}), elimination half-life ($t_{1/2}$), and the AUC from zero to infinity (AUC_{inf}) for all Pt species. Clearance (Cl) and volume of distribution (V_z) were calculated for total plasma Pt.

RESULTS

Patient characteristics

The first patient was dosed on 15 May 2006 and the last study exit visit occurred on 6 February 2008. In total, 17 patients were enrolled and each received at least one dose of NC-6004, representing the intention-to-treat population. Demographic characteristics of patients are summarised in Table 2. All recruited patients were Caucasian, with a median height of 170.0 cm and a median weight of 73.0 kg. Cancer history of patients is summarised in Table 3. The range of tumour types was large, with no specific tumour type represented more across the different groups. Tumour stage was similar between the dosing cohorts.

Dosing and toxicity

The process for dose escalation is shown in Table 3. In total, 41 doses were administered to 17 patients. The maximum number of treatments was four cycles in three patients, and the mean number of administrations per patient was 2.4 cycles. Dose escalation started at $10\,\mathrm{mg\,m^{-2}}$ and was increased up to $40\,\mathrm{mg\,m^{-2}}$ following the accelerated titration method. Owing to grade 2 renal toxicity in cycle 1 of a patient at $40\,\mathrm{mg\,m^{-2}}$, reported as a serious adverse event (SAE), the study entered stage 2 with a dose escalation up to $120\,\mathrm{mg\,m^{-2}}$ according to modified Fibonacci method.

Infusion-related adverse events are summarised in Table 4. NC-6004 injection was well tolerated in terms of haematological toxicities. Thus, one episode of grade 3 thrombocytopenia at $10\,\mathrm{mg\,m^{-2}}$ and grade 1 thrombocytopenia at $90\,\mathrm{mg\,m^{-2}}$ only were observed (not DLTs). For non-haematological toxicity, the most frequent related adverse events were fatigue (52.9%), anorexia and nausea (47.1%), vomiting (41.2%), and hypersensitivity reaction and renal impairment (35.3%). Significant cisplatin-related otoxicity and neurotoxicity were not observed at any dose level.

Table 2 Patient characteristics

	NC-6004 dose level (in $\mathrm{mg\,m^{-2}}$)						
	10	20	40	60	90	120	Total
n	1	1	3	3	6	3	17
Age (years)							
Range	55	63	45–65	45–56	48–80	40–71	40–80
Sex							
Male	1	0	2	2	4	1	10
Female	0	1	1	1	2	2	7
ECOG PS[a]							
0	1	0	2	1	4	2	10
1	0	0	1	0	1	1	3
2	0	1	0	1	1	0	3
Previous treatment							
Chemotherapy	1	1	3	3	5	2	15
Surgery	0	0	3	3	3	3	12
Radiotherapy	0	1	1	2	0	3	7
Other therapies for cancer (targeted therapy, immunotherapy, or epigenetic therapy)	0	0	0	2	1	2	5

Abbreviation: ECOG PS = Eastern Cooperative Oncology Group performance status. [a]For one patient at $60\,\mathrm{mg\,m^{-2}}$, ECOG PS was not assessed at screening, but was assessed at day 1 before infusion.

One out of six patients at $90\,\mathrm{mg\,m^{-2}}$ experienced grade 3 fatigue in cycle 1 (DLT). One out of three patients at $60\,\mathrm{mg\,m^{-2}}$ had grade 3 vomiting in cycle 1, and one patient in each 60, 90, and $120\,\mathrm{mg\,m^{-2}}$ developed grade 3 hypersensitivity reaction (not DLTs). The clinical signs and symptoms of hypersensitivity reactions to NC-6004 were urticarial rash, dizziness, sweating, cough, dyspnoea, hypotension, tingling, swelling of tongue, lip, and pharynx, tightness in chest, and burning sensation, some of which are typical reactions for Pt, and they always developed after a minimum of two cycles of NC-6004. Other infusion-related toxicities were grade 2 or lower. Despite the implementation of post hydration (from $40\,\mathrm{mg\,m^{-2}}$ onwards) and hypersensitivity prophylaxis (from $90\,\mathrm{mg\,m^{-2}}$ onwards), grade 2 renal toxicity accompanied by a reduction in dose and/or delay in dose for 1 week was still observed at 90 and $120\,\mathrm{mg\,m^{-2}}$, and grade 2 and 3 hypersensitivity reactions (SAEs) also developed at $120\,\mathrm{mg\,m^{-2}}$. Following these events, it was considered that adding further patients or increasing the dose level would not be reasonable, and the study was discontinued at dosage level of $120\,\mathrm{mg\,m^{-2}}$. As the effect on renal function at $90\,\mathrm{mg\,m^{-2}}$ dosage was less marked than that observed at $120\,\mathrm{mg\,m^{-2}}$, the $120\,\mathrm{mg\,m^{-2}}$ dosage was considered to be the MTD, and the RD of NC-6004 as monotherapy for further studies was therefore estimated to be $90\,\mathrm{mg\,m^{-2}}$, although renal toxicity and hypersensitivity reactions were not defined as potential DLT per protocol.

Therapeutic response

Best overall response calculated by RECIST is shown in Table 3. No patient was assessed as complete response or partial response. Seven patients (41.2%) were evaluated as having had a stable disease (SD) for longer than 4 weeks at the time of the study completion, even though six of these had advanced Stage IV solid tumours. It should be noted that only two out of eight patients (25%) at the dose levels from 10 to $60\,\mathrm{mg\,m^{-2}}$ had a best response of SD, however the SD ratios at 90 and $120\,\mathrm{mg\,m^{-2}}$ were 50 and 67% respectively, suggesting that the efficacy of NC-6004 is more pronounced at higher dose levels. Overall, 14 patients (82.4%) died or experienced tumour progression, and median progression-free survival time was 49 days.

Table 3 Process for dose escalation

Dose (mg m^{-2})	Patient no.	Primary tumour (stage)	Cycles received	No. of DLT	Events	Best overall response
Stage 1						
10	101	Lung (IV)	3	0	Hypersensitivity reaction at cycle 3 (previous cisplatin therapy)	SD
20	102	Lung (IV)	2	0		PD
40	103	Colon (IV)	1	0	Grade 2 reduced renal function at cycle 1 (SAE). Cohort was expanded with two more patients.	PD
	204	Hepatic cell (IV)	4	0		SD
	105	Colon (IV)	2	0	Grade 1 reduced renal function at cycle 1. Hydration was implemented for the rest of study.	PD
Stage 2						
60	106	Mesothelioma (IIIA)	2	0	Hypersensitivity reaction at cycle 2 (previous carboplatin therapy).	PD
	207	Colon (IV)	2	0	Hypersensitivity reaction at cycle 2 (previous oxaliplatin therapy).	PD
	108	Oesophagus (IV)	2	0		NE
90	209	Pancreas (IIA)	4	0	Hypersensitivity reaction at cycle 4 (Pt-naïve). Prophylactic treatment was implemented for the rest of study.	SD
	110	Oesophagus (IV)	2	0	Grade 2 reduced renal function at cycle 1.	PD
	112	GIST (IV)	2	0	Grade 2 reduced renal function at cycle 1. Cohort was expanded with three more patients.	PD
	113	Lung (IV)	2	0		SD
	114	Pancreas (IV)	2	1	Grade 3 fatigue at cycle 1 (DLT).	SD
	215	Colon (IV)	2	0		PD
120	216	Melanoma (IV)	2	0	Grade 2 reduced renal function at cycle 1.	PD
	117	Melanoma (IV)	4	0	Grade 2 reduced renal function at cycle 1. Hypersensitivity reaction at cycle 4 (SAE) (Pt-naïve).	SD
	218	Renal cell (IV)	3	0	Hypersensitivity reaction at cycle 3 (SAE) (Pt-naïve).	SD

Abbreviations: DLT = dose-limiting toxicity; GIST = gastrointestinal stromal tumour; PD = progressive disease; Pt = platinum; NE = not estimated; SAE = serious adverse event; SD = stable disease.

Table 4 Summary of all related adverse events

	NC-6004 dose level (in mg m^{-2})						
	10	**20**	**40**	**60**	**90**	**120**	**Total**
n	1	1	3	3	6	3	17
Haematological toxicity							
Blood and lymphatic system disorders							
Thrombocytopenia	1	0	0	0	1	0	2
Non-haematological toxicity							
Gastrointestinal disorder							
Constipation	0	0	0	0	0	1	1
Dry mouth	0	0	0	1	0	0	1
Nausea	0	1	1	1	4	1	8
Paraesthesia oral	0	0	0	0	0	1	1
Tongue ulceration	0	0	0	0	1	0	1
Vomiting	0	0	1	1	4	1	7
General disorder and administration site conditions							
Fatigue	1	1	0	1	4	2	9
Infusion site reaction	0	1	0	0	0	0	1
Malaise	0	0	0	0	0	1	1
Immune system disorders							
Hypersensitivity	1	0	0	2	1	2	6
Metabolism and nutrition disorders							
Anorexia	0	0	2	1	4	1	8
Decreased appetite	0	0	0	1	0	0	1
Dehydration	0	0	0	0	1	0	1
Hypomagnesemia	0	0	0	0	1	0	1
Nervous system disorder							
Dizziness	0	0	0	0	0	1	1
Neuropathy peripheral	1	0	0	1	0	0	2
Peripheral sensory neuropathy	0	0	0	0	1	0	1
Renal and urinary disorder							
Renal impairment	0	0	2	0	2	2	6
Skin and subcutaneous tissue disorder							
Alopecia	0	0	0	0	0	1	1
Rash	0	0	0	0	0	1	1

Table 5 Pharmacokinetic parameters per cohort for total, micellar, and ultrafiltrable Pt of NC-6004 (mean ± s.d.)

Analyte	Dose (mg m^{-2})	T_{max} (h)	C_{max} (μg ml^{-1})	$t_{1/2}$ (h)	AUC$_{inf}$ (h μg ml^{-1})	V_z (l)	Cl (ml h^{-1})
Total Pt	10	4.0	5.70	24	234	3.0	85
	20	5.4	12.20	20	492	2.0	68
	40	2.0 ± 0.1	25.9 ± 2.4	62 ± 18	1135 ± 78	5.5 ± 2.0	62 ± 11
	60	2.7 ± 1.2	29.9 ± 13.8	93 ± 41	1354 ± 638	6.7 ± 0.5	107 ± 69
	90	5.2 ± 2.2	60.8 ± 12.5	129 ± 40	2836 ± 554	11.8 ± 6.9	61 ± 20
	120	4.4 ± 2.5	85.4 ± 10.8	158 ± 48	4377 ± 563	10.9 ± 3.8	48 ± 9
Micellar Pt	10	—[a]	—[a]	—[a]	—[a]		
	20	6.4	8.90	16	237		
	40	2.0 ± 0.1	13.9 ± 10.4	67 ± 56	509 ± 204		
	60	5.0 ± 1.7	14.4 ± 7.3	18 ± 7	385 ± 153		
	90	4.8 ± 2.4	42.4 ± 20.3	39 ± 27	1579 ± 939		
	120	3.1 ± 1.5	84.6 ± 8.1	87 ± 37	3857 ± 1171		
UF Pt	10	48.7	0.009	114	1.7		
	20	23.5	0.022	71	2.5		
	40	24.0 ± 0.1	0.045 ± 0.014	141 ± 126	4.7 ± 2.1		
	60	26.5 ± 20.9	0.096 ± 0.022	114 ± 47	13.2 ± 5.8		
	90[b]	20.5 ± 7.6	0.205 ± 0.114	123 ± 44	22.6 ± 10.0		
	120[c]	26.4	0.131	115	22.9		

Abbreviations: AUC$_{inf}$ = area under concentration–time curve from zero to infinity; Cmax = maximum concentration; Cl = clearance; Pt = platinum; QC = quality control; T_{max} = time to maximum concentration; UF Pt = ultrafilterable platinum; Vz = volume of distribution. [a]Data not valid – QCs out with acceptance limit. [b]1 data was not valid – QCs out with acceptance limit. [c]2 data were not valid – QCs out with acceptance limit.

Pharmacokinetics

Pharmacokinetic parameters for Pt measured per cohort in the three different matrices are shown in Table 5. A typical plasma concentration–time profile is also shown in Figure 3.

Pharmacokinetics of total plasma Pt was characterised by longer $t_{1/2}$, and higher C_{max} and AUC$_{inf}$ with smaller V_z and Cl compared with those of cisplatin, indicating that the blood circulation of cisplatin was prolonged by the incorporation into the micelles. Thus, the C_{max} and AUC$_{inf}$ of NC-6004 at 120 mg m^{-2} were approximately 11-fold higher than those of cisplatin at an equivalent dose (Kitajima et al, 1987). The $t_{1/2}$ of NC-6004 at 120 mg m^{-2} was longer than that of cisplatin at an equivalent dose, 14.6 min for the initial phase and 73.8 h for the terminal phase (Kitajima et al, 1987). The V_z and Cl of NC-6004 were smaller than those of cisplatin, 521 and 350 ml h^{-1}, respectively (Calvert et al, 1993). The AUC$_{inf}$ and C_{max} of NC-6004 increased in a dose-dependent manner, and there was no apparent change in Cl with increasing dose.

For the gel-filterable Pt (intact micellar formulation), the T_{max} was similar to that of total plasma Pt, the $t_{1/2}$ generally mirrored that of total plasma Pt, and the C_{max} and AUC$_{inf}$ values were approximately 88% of those of total plasma Pt.

For the ultrafilterable Pt (active species including cisplatin), the C_{max} at 120 mg m^{-2} was 34-fold lower than that of non-protein-bound cisplatin after the administration of an equivalent dose of cisplatin (Kitajima et al, 1987), which might be responsible for the lower incidence of toxicity compared with that associated with cisplatin therapy. Conversely, $t_{1/2}$ and AUC$_{inf}$ at 120 mg m^{-2} of NC-6004 were 230-fold and 8.5-fold larger, respectively, than those of non-protein-bound cisplatin after the administration of an equivalent dose of cisplatin (Kitajima et al, 1987). The persistence of active Pt species might indicate an improved efficacy of NC-6004. Furthermore, T_{max} (24 h or greater) was delayed compared with that of total plasma Pt or gel-filterable Pt, suggesting that NC-6004 provides a delayed and sustained release of potentially active Pt species after the administration period.

DISCUSSION

NC-6004 was well tolerated with minimal nephrotoxicity and no significant myelosuppression, ototoxicity, emesis, or neurotoxicity, but a higher rate of hypersensitivity reactions than predicted. No DLT per protocol was seen at doses up to 90 mg m^{-2} where 1 DLT
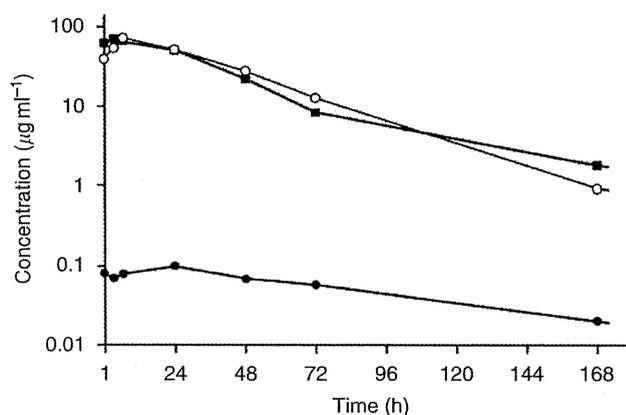
Figure 3 Plasma Pt concentration–time curve from a patient treated at 90 mg m^{-2} of NC-6004. ■, total Pt, O, gel-filterable Pt, ●, ultrafilterable Pt.

(grade 3 fatigue) was experienced by one out of six patients, and no further DLT per protocol was seen at 120 mg m^{-2} when the study was discontinued. In general, the toxicities of NC-6004 were less severe and less frequent compared with cisplatin, particularly nausea/vomiting, anorexia, alopecia, and haematological toxicity.

In this study, dose delays/reductions were mainly due to effects on renal function. Despite the introduction of 1 to 1.5 l of fluid over 2 h, following NC-6004 administration, rising creatinine and/ or reduction in estimated creatinine Cl or ^{51}Cr-EDTA Cl affected two out of six patients at 90 mg m^{-2} and two out of three patients at 120 mg m^{-2}, although the creatinine level returned to baseline in 2 weeks. Cisplatin therapy requires a total 8 h hydration, comprising 1–21 over 4 h of hydration, both before and after the administration of cisplatin, to prevent nephrotoxicity. Another potential advantage of NC-6004 over cisplatin is, therefore, the reduced need for hydration, and that renal impairment was kept to minimum by modest hydration. Whether hydration is absolutely necessary for NC-6004 therapy to reduce the incidence of renal impairment remains to be assessed in a future trial.

Dose interruptions due to toxicity in this study were all related to hypersensitivity reactions, which occurred unpredictably at four

out of six dose levels (10, 60, 90, and 120 mg m^{-2}) in six patients. The first three patients had previous Pt therapy and the last three patients were Pt-naïve, thus, the occurrence of hypersensitivity reaction depends on neither dose level nor the previous Pt exposure. The use of a prophylactic regimen of dexamethasone, ranitidine, and chlorphenamine, previously described, was not sufficient to prevent hypersensitivity reactions in two patients at 120 mg m^{-2}, therefore a more stringent prophylactic regimen (Kwon et al, 2002) might be necessary. As most of the patients recruited in this Phase I study progressed by the end of cycle 2, and hypersensitivity reactions developed after a minimum of two cycles of NC-6004, despite the pre-medication, it was considered that this phase I study was not the appropriate setting to assess alternative pre-medication strategies. Therefore, the study was discontinued, so that this problem could be assessed in a future trial. In preclinical studies, the antigenicity of NC-6004 was examined compared with cisplatin, polymer vehicle, polymer-bound cisplatin (not in a micelle form), and cisplatin – plasma protein complex. The results indicated that cisplatin and polymer vehicle are not antigenic, and the highest extent of antigenicity observed was in cisplatin – plasma protein complex, followed by NC-6004 and then polymer-bound cisplatin (not in a micelle form). This suggests that the hypersensitivity reaction to NC-6004 may have been due to plasma protein-bound cisplatin, which is formed by rapid binding of plasma protein to released cisplatin, which then circulates in the blood for a prolonged period. However, the mechanism has not yet been fully clarified.

Taking account of the incidence of hypersensitivity reaction and renal impairment, 120 mg m^{-2} was considered to be close to the MTD, such that 90 mg m^{-2} was most likely the RD for monotherapy for future studies, although the definition per protocol of the MTD was not actually reached.

In spite of the patients generally being heavily pretreated, some evidence of disease stabilisation was seen, and seven patients demonstrated SD after 6 weeks of treatment. Efficacy will be further assessed in a future trial.

The pharmacokinetic analysis indicated the prolonged circulation of NC-6004 in the blood, and delayed and sustained release of potentially active Pt species after the administration of NC-6004. More importantly, the observed lower C_{max} for ultrafilterable Pt compared with that of non-protein-bound cisplatin, after the cisplatin injection, might result in the reduction of cisplatin-related toxicity. Furthermore, the higher AUC_{inf} and $t_{1/2}$ for ultra-filterable Pt compared with that of non-protein-bound cisplatin after the cisplatin injection might enhance the efficacy of NC-6004. However, an increase in the AUC of plasma protein-bound cisplatin because of rapid binding of plasma protein to released cisplatin might result in a higher risk of hypersensitivity reaction.

In conclusion, this Phase I study has confirmed that NC-6004 exhibits pharmacokinetic characteristics completely different from those of cisplatin, resulting in the reduction of cisplatin-related toxicity and the improvement of patient's quality of life so that the patients can take therapy without hospitalisation for hydration and treatment of cisplatin-related toxicities. The data obtained from this study are believed to open new avenues for the use of this micellar formulation in the clinic. The assessment of the most appropriate prophylactic regimen for hypersensitivity reactions, whether hydration is necessary and of efficacy are now underway in ongoing NC-6004 studies.

REFERENCES

Calvert H, Judson I, Van der Vijgh WJF (1993) Platinum complexes in cancer medicine: pharmacokinetics and pharmacodynamics in relation to toxicity and therapeutic activity. *Pharmacokinet Cancer Chemother* 17: 189–217

Hartmann JT, Lipp H-P (2003) Toxicity of platinum compounds. *Expert Opin Pharmacother* 4: 889–901

Judson I, Kelland LR (2000) New developments and approaches in the platinum arena. *Drugs* 59(Suppl. 4): 29–36

Kartalou M, Essigmann JM (2001) Mechanisms of resistance to cisplatin. *Mutat Res* 478: 23–43

Kelland LR, Sharp SY (1999) Platinum compounds in cancer therapy. *Curr Opin Oncol Endocrine Metabolic Invest Drugs* 1: 380–385

Kitajima K, Fukuoka M, Kobayashi S, Kusunoki Y, Takada M, Negoro S, Matsui K, Sakai N, Ryu S, Takifuji N (1987) Studies on appropriate administration of cisplatin based on pharmacokinetics and toxicity. *Jpn J Cancer Chemother* 14: 2517–2523

Kwon JS, Elit L, Finn M, Hirte H, Mazurka J, Moens F, Trim K (2002) A comparison of two prophylactic regimens for hypersensitivity reactions to paclitaxel. *Gynecol Oncol* 84: 420–425

Maeda H (2001) The enhanced permeability and retention (EPR) effect in tumor vasculature: the key role of tumor-selective macromolecular drug targeting. *Advan Enzyme Regul* 41: 189–207

Maeda H, Matsumura Y (1989) Tumoritropic and lymphotropic principles of macromolecular drugs. *Crit Rev Ther Drug Carrier Syst* 6: 193–210

Maeda H, Wu J, Sawa T, Matsumura Y, Hori K (2000) Tumor vascular permeability and the EPR effect in macromolecular therapeutics: a review. *J Control Rel* 65: 271–284

Matsumura Y, Maeda H (1986) A new concept for macromolecular therapeutics in cancer chemotherapy: mechanism of tumoritropic accumulation of proteins and the antitumor agent smancs. *Cancer Res* 46: 6387–6392

Nishiyama N, Kataoka K (2001a) Preparation and characterization of size-controlled polymeric micelle containing cis-dichlorodiammineplatinum (II) in the core. *J Control Rel* 74: 83–94

Nishiyama N, Kato Y, Sugiyama Y, Kataoka K (2001b) Cisplatin-loaded polymer-metal complex micelle with time-modulated decaying property as a novel drug delivery system. *Pharm Res* 18: 1035–1041

Nishiyama N, Okazaki S, Cabral H, Miyamoto M, Kato Y, Sugiyama Y, Nishio K, Matsumura Y, Kataoka K (2003) Novel cisplatin-incorporated polymeric micelles can eradicate solid tumors in mice. *Cancer Res* 63: 8977–8983

Nishiyama N, Yokoyama M, Aoyagi T, Okano T, Sakurai Y, Kataoka K (1999) Preparation and characterization of self-assembled polymer-metal complex micelle from cis-dichlorodiammineplatinum (II) and poly(ethylene glycol)-poly(α,β-aspartic acid) block copolymer in an aqueous medium. *Langmuir* 15: 377–383

Pinzani V, Bressolle F, Hang IJ, Galtier M, Balyac JP, Balmes P (1994) Cisplatin-induced renal toxicity and toxicity-modulating strategies: a review. *Cancer Chemother Pharmacol* 35: 1–9

Sharp SY, O'Neill CF, Rogers P, Boxall FE, Kelland LR (2002) Retention of activity by the new generation platinum agent AMD0473 in four human tumour cell lines possessing acquired resistance to oxaliplatin. *Eur J Cancer* 38: 2309–2315

Uchino H, Matsumura Y, Negishi T, Koizumi F, Hayashi T, Honda T, Nishiyama N, Kataoka K, Naito S, Kakizoe T (2005) Cisplatin-incorporating polymeric micelles (NC-6004) can reduce nephrotoxicity and neurotoxicity of cisplatin in rats. *Br J Cancer* 93: 678–687

Yokoyama M, Okano T, Sakurai Y, Suwa S, Kataoka K (1996) Introduction of cisplatin into polymeric micelle. *J Control Rel* 39: 351–356

New concept of cytotoxic immunoconjugate therapy targeting cancer-induced fibrin clots

Masahiro Yasunaga,[1] Shino Manabe[2] and Yasuhiro Matsumura[1,3]

[1]Investigative Treatment Division, Research Center for Innovative Oncology, National Cancer Center Hospital East, Kashiwa, Chiba; [2]Synthetic Cellular Chemistry Laboratory, RIKEN Advanced Science Institute, Wako, Saitama, Japan

Fibrin clots in non-malignant conditions form only at the onset or during the active stage of disease and disappear within a few weeks as a result of plasmin digestion or replacement with collagen. In contrast, fibrin clot formation and subsequent replacement with collagen in cancer persist for as long as the cancer cells survive in the body. We developed an anti-fibrin chimeric antibody that reacts with fibrin only, and not fibrinogen (the precursor of fibrin), and then attached an anticancer agent (ACA) to the antibody. Thus, the immunoconjugate did not create an immune complex in the blood stream and was selectively accumulated to fibrin clots in the tumor stroma to create a scaffold, from which effective sustained release of the ACA occurred. In a mouse model, the ACA diffused throughout the tumor tissue to damage both tumor cells and vessels, resulting in potent antitumor activity in stroma-rich spontaneous tumors. This new cancer stroma-targeting therapy may result in an increased duration of drug exposure and be a highly effective new therapy, particularly for refractory, stroma-rich cancers. (*Cancer Sci* 2011; 102: 1396–1402)

L ow molecular weight (LMW) anticancer agents (ACA), including molecular targeting agents, are very efficient cytocidal agents in the closed space of a monolayer culture dish. The antitumor effects of these agents are determined using subcutaneous tumor xenografts, the pathophysiological features of which are far removed from those of general human cancers. Although there have been numerous reports of genetic and phenotype changes in tumors, there are no pivotal changes in tumor cells that distinguish them from normal dividing cells.[1–6] Unlike the situation in culture, following the administration of LMW ACA to patients, these agents are cleared quickly from tumors in the body. In addition, the ACA are distributed throughout the body, resulting in serious side effects.[7] To overcome off-target effects caused by LMW ACA, immunoconjugate therapy was developed in which an ACA or toxin is conjugated to a cancer cell-specific mAb, which is too large to pass through a normal vessel wall but can extravasate from leaky tumor vessels and accumulate selectively in tumor tissue.[8–12] The kinetics of drug distribution within tumors are considered to be a function of interstitial conductivity, which is determined by the quantity and density of the extracellular matrix (e.g. proteoglycan, fibronectin) and fibrosis (e.g. fibrin, collagen fibers) in the stroma.[13–16] Most human solid tumors have abundant stroma that hinders the distribution of high molecular weight (HMW) agents, including ACA-conjugated antibodies. Consequently, the tissue becomes a barrier preventing the immunoconjugates from attacking cancer cells.[14–16] This led us to design a novel alternative antitumor strategy that turned this apparent handicap into an asset.

In the 19th century, French surgeon Armand Trousseau described, for the first time, thrombophlebitis in patients with stomach cancer.[17] Today, a large body of clinical evidence supports the conclusion that abnormal coagulation followed by

fibrin formation occurs in a variety of cancers.[18,19] Different types of tumor cells express the tissue factor that is known to be a cell surface membrane protein and a trigger of the extrinsic coagulation pathway.[18,20] Above all, any malignant tumor erodes adjacent normal or tumor vessels, resulting in microscopic hemorrhages within or adjacent to cancer tissues; fibrin clots should form immediately *in situ* to stop the bleeding. Although fibrin clot formation also occurs in non-malignant disorders, such as cardiac or brain infarction, injuries, and active rheumatoid arthritis, these fibrin clots form only at the onset or during the active stage of the disease. Moreover, these fibrin clots disappear within a few weeks as a result of plasmin digestion or replacement with collagen fibers. In tumor tissues, the fibrin clots are replaced by collagenous stroma in a process similar to that in normal wound healing and other non-malignant diseases.[13] However, unlike non-malignant conditions, fibrin clot formation in cancer tissues lasts for as long as the cancer cells survive in the body. Therefore, unlike growth factors and tyrosine kinases, fibrin clots are pathophysiologically specific for tumors. In that context, we developed an mAb against fibrin to target the tumor stroma. In addition, we exploited the newly developed specialized immunoconjugate linker to conjugate the anti-fibrin mAb with an ACA.

Materials and Methods

Antibodies. A hybridoma producing anti-fibrinogen (mouse IgG clone K88-3) or anti-fibrin antibody (mouse IgM clone 102-10) was established using myeloma cells (P3U1) and lymph node cells from the mouse with immunizing human fibrinogen (Sigma, St. Louis, MO, USA) or fibrin, with the latter converted from fibrinogen by thrombin (Sigma) cleavage. Heavy chain variable and kappa light chain variable cDNAs were cloned into the vector for human IgG1 expression. The vectors were transfected into Chinese hamster ovary (CHO) cells (Riken Bioresource Center, Tsukuba, Japan) and a stable clone (humanized IgG, clone 102-10) was isolated.

Camptothecin-11 (CPT-11; irinotecan) and SN-38 were purchased from Tokyo Chemical Industry (Tokyo, Japan) and Yakult (Tokyo, Japan), respectively.

In vivo **imaging and immunohistochemistry.** Antibodies were conjugated with Alexa-647 (Invitrogen, Carlsbad, CA, USA) according to the manufacturer's instructions. *In vivo* fluorescence imaging was performed using a confocal fluorescence microscope (A1R; Nikon, Tokyo, Japan) or a small animal imaging system (OV110; Olympus, Tokyo, Japan). For immunohistochemistry, anti-fibrin IgM was incubated with Alexa 488-labeled anti-mouse IgG (Invitrogen) as a secondary antibody. The unbound antibodies were blocked with mouse serum (Dako, Glostrup, Denmark). First, samples were incubated for 30 minutes at room temperature in the dark with the

3To whom correspondence should be addressed.
E-mail: yhmatsum@east.ncc.go.jp

immunocomplex (anti-fibrin IgM and Alexa 488 secondary Ab), anti-cytokeratin (Abcam, Cambridge, UK), or anti-CD31 (Becton Dickinson, Franklin Lakes, NJ, USA). Then, samples were incubated for 60 minutes at room temperature in the dark with Alexa 488-, 555- or 647-labeled anti-rabbit IgG (Invitrogen) or phycoerythrin (PE)-labeled anti-rat IgG (Jackson ImmunoResearch, West Grove, PA, USA). Fluorescence images were obtained using a digital high-definition microscopic system (BZ-9000; Keyence, Osaka, Japan).

Synthesis of the SN-38 derivative linker. A detailed description of the synthesis of the linker is provided online as supplementary material for this paper (Data S1). Briefly, PEG was purchased from Quanta BioDesign (Powell, OH, USA) and Merck (Whitehouse Station, NJ, USA). Reagents and solvents were purchased from Sigma and Kanto (Tokyo, Japan). The final structure was composed of one maleimide for the attachment of mAb, one PEG_{12} spacer and three PEG_{27} ester bonds for attachment of three SN-38 molecules. The structure and purity of the chemically synthesized materials were determined by 400-MHz ^{1}H-NMR and ^{13}C-NMR (NMR ECX-400 or NMR AL; JEOL Ltd., Tokyo, Japan) and mass spectrometry (MS AXIMA; Shimadzu, Kyoto, Japan). The derivatives were resolved in DMSO (Sigma).

Immunoconjugate. The interchain disulfides of the Abs were first reduced with 10 mM DTT (Sigma). The number of free thiols was quantified using 5,5'-dithiobis 2-nitrobenzoic acid (DTNB; Wako Pure Chemical Industries, Osaka, Japan). Reduced Abs were purified by gel filtration (Amicon Ultra Centrifugal Filter Devices; Millipore, Billerica, MA, USA) and reacted with linker SN-38 derivative in PBS containing 5 mM EDTA (pH 6) at room temperature for 1 h, then at 4°C overnight. The SN-38-conjugated Abs were purified by gel filtration (Millipore). The concentration of Ab–prodrug conjugates was determined using the Bradford method (Bio-Rad Protein Assay, 500-0006JA; Bio-Rad, Hercules, CA, USA). The number of residual thiols was quantified with DTNB. The ratio of each drug (SN-38)/Ab was determined by comparison of the number of free and residual thiols.

High-performance liquid chromatography. The kinetics of release of SN-38 from the immunoconjugate was investigated *in vitro* at 37°C in 5% glucose (pH 4.6), PBS (pH 7.4), or mouse serum. Whole tumor tissues were mixed with 0.1 M glycine–HCl buffer (pH 3.0)/methanol (5 w/w%) and then homogenized. Samples (100 μL) were then mixed with 20 μL of 1 mM phosphoric acid/methanol (1:1), 40 μL ultrapure water, and 60 μL camptothecin solution (Sigma) as an internal standard. Reaction solutions and plasma were mixed with 0.1 M HCl at 50% (w/w). The samples (50 μL) were then mixed with 20 μL of 1 mM phosphoric acid in methanol (1:1) and 100 μL camptothecin as an internal standard. Samples were vortexed for 10 s and filtered through an Ultrafree-MC (Millipore). To detect immunoconjugated SN-38, samples (20 μL plasma, 100 μL tumor) were diluted with 20 μL methanol (50% w/w) and 20 μL NaOH (0.7 M). After incubation for 15 minutes at room temperature, 20 μL HCl (0.7 M) and 60 μL internal standard solution were added to the samples, and the hydrolysate was then filtered. Reverse-phase HPLC was performed at 35°C on a Mightysil RP-18 GP column (150 × 4.6 mm; Kanto). Samples were injected into an Alliance Waters 2795 HPLC system (Waters, Milford, MA, USA) equipped with a Waters 2475 multi λ fluorescence detector at excitation and emission wavelengths of 365 and 540 nm, respectively, for SN-38 or 365 and 430 nm, respectively, for CPT-11.

Animal model and antitumor effects. Chemical skin carcinogenesis was induced in female FVB/N mice (CLEA, Tokyo, Japan) as described previously.[21,22] Briefly, a single application of 7,12-dimethylbenz[α]anthracene (DMBA; 250 μg/mL in acetone; Sigma) was applied to the shaved dorsal skin of mice.

After 1 week, phorbol 12-myristate 13-acetate (PMA); 25 μg/mL in acetone; Sigma) was applied weekly (for a total of 32 times). Carcinoma was determined on the basis of the clinical appearance of characteristic features, according to the previous report.[22] Histological analysis was performed to confirm the diagnosis of carcinoma based on clinical appearance (Fig. 1A). Tumor volume was calculated as (length × width^2)/2. When the mean size of tumors that grew continuously over a period of 3 weeks reached approximately 70 mm^3, the tumors were randomly divided into three groups comprising five tumors in each group such that there was no significant difference in tumor size among them. Immunoconjugates were administered on Days 0, 7, 14, and 21 by tail vein injection. An injection dose of antibody–SN-38 prodrug equal to an SN-38 dose of 13.3 mg/kg was determined by calculations based on the drug (SN-38)/antibody ratio for each drug. Statistical analyses of both antitumor effects and changes in body weight were performed using ANOVA.

All animal procedures were performed in compliance with the *Guidelines for the Care and Use of Experimental Animals* established by the Committee for Animal Experimentation of the National Cancer Center. These guidelines meet the ethical standards required by law and also comply with the guidelines for the use of experimental animals in Japan (http://www.scj.go.jp/ja/info/kohyo/pdf/kohyo-20-k16-2.pdf).

In vivo fiber confocal fluorescence microscopy. For visualization of tumor vessels, 400 μg FITC–dextran (250 kDa; Sigma) was injected into tumor-bearing mice before and 5 days after treatment with the immunoconjugate using the imaging system Cellvizio (Mauna Kea Technologies, Paris, France).[23] Mean vessel diameter, total vessel length, and total area were estimated at six different sites within the tumor before and after treatment using ImageCell software (Mauna Kea Technologies). The length of functional capillary density (FCD) was calculated as (total vessel length/total area). Statistical analyses were performed using Student's *t*-test.

Results

Preparation of anti-fibrin chimeric IgG for stroma targeting. We developed an mAb against fibrin, which is abundant in the stroma of human solid tumors. After extensive screening using two ELISA sets, one for human fibrinogen (the precursor of fibrin that is present physiologically) and the other for human fibrin (which is formed only in some abnormal conditions), we successfully developed an mAb that reacted with human fibrin only and not with human fibrinogen. However, because the mAb obtained was IgM, it was converted into the human IgG format for clinical application using an antibody engineering technique. Another advantage of the mAb was that the mAb cross-reacted with mouse fibrin and not with mouse fibrinogen (Fig. 1B). Chemically induced mouse cutaneous cancer was selected as an appropriate experimental model in which to evaluate the therapeutic effects of our immunoconjugate chemotherapy because this spontaneous carcinogenetic model has marked fibrin deposition and abundant interstitial tissue, as in human cancer (Fig. 1A) and unlike human tumor xenografts, which have fewer fibrin clots and less interstitial tissue.[24,25] In addition, the spontaneous tumors exhibit very slow growth, which is similar to the condition in general human cancer but not in the xenografts.

Using real-time *in vivo* confocal microscope imaging, the anti-fibrin chimeric IgG (AFCA) was found to be distributed in the extravascular component 1 h after injection, whereas the leakage of anti-fibrin IgM from the vessels was so restricted that obvious extravascular distribution was not observed over the same period (Fig. 1C). Using systemic *in vivo* imaging, anti-fibrin IgM, anti-fibrin IgG, and anti-fibrinogen IgG were delivered and retained in the tumor until Day 3, utilizing leaky tumor
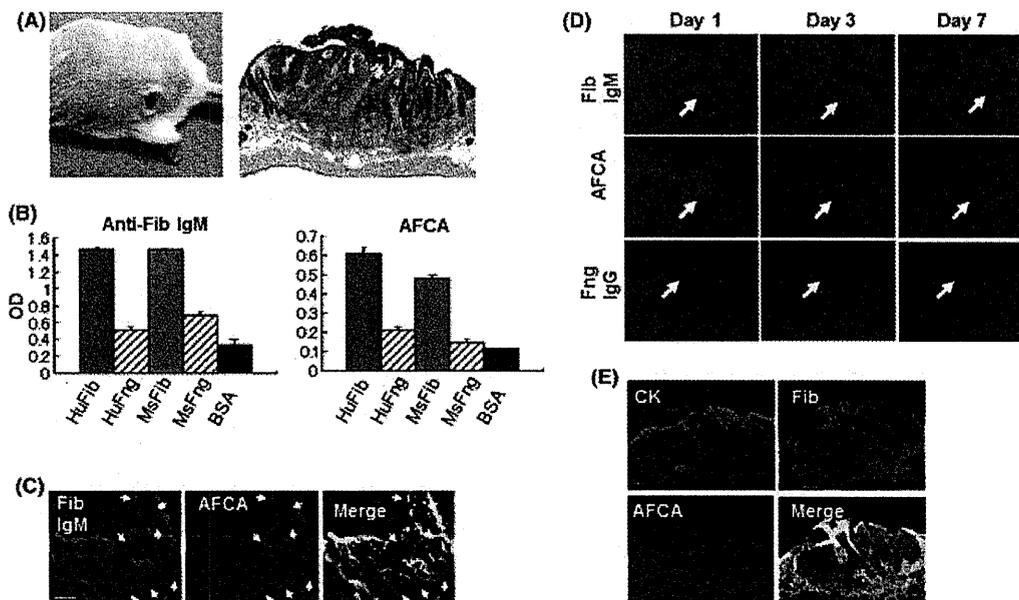
Fig. 1. Preparation and characterization of the anti-fibrin antibody. (A) Chemical skin carcinogenesis. A mouse bearing a tumor (left) and hematoxylin-eosin staining (right) of the tumor. (B) Both anti-fibrin (Fib) IgM and its chimeric IgG (AFCA) were shown to recognize human (Hu) and mouse (Ms) fibrin, but not their fibrinogen (Fng), by ELISA. OD, optimal density. (C) In vivo confocal microscope imaging showing leakage of Alexa 488-labeled anti-fibrin IgM (left; green) and Alexa 647-labeled AFCA (middle; red) from tumor vessels 1 h after injection. Arrows indicate the area into which the AFCA has leaked (right; red in Merge). Scale bar, 100 μm. (D) In vivo systemic imaging analysis of Alexa 647-labeled anti-fibrin IgM (upper), AFCA (middle), or anti-fibrinogen mAb (lower) on Days 1, 3, and 7 after injection. Arrows indicate each tumor position. (E) Intratumoral distribution of injected fluorescent AFCA (lower left; red) was examined 24 h after injection. Immunohistochemistry with anti-cytokeratin (upper left; light-blue) or anti-fibrin (upper right; green). Yellow indicates the overlap of injected anti-fibrin IgG and deposited fibrin (lower right). Scale bar, 100 μm.

vessels.[10,11] The accumulation of anti-fibrin IgM and anti-fibrinogen IgG was weak and they were eliminated by Day 7; however, on Day 7, AFCA was still highly retained within the tumor (Fig. 1D). Therefore, we used AFCA as a vehicle for drug delivery, providing high accumulation and long-term retention in the tumor. Investigating the intratumoral distribution of AFCA, we found that it was observed mainly in fibrin-positive stroma and was rarely seen in cytokeratin-positive tumor cell areas (Fig. 1E). Thus, we succeeded in developing an anti-fibrin IgG for targeting the tumor stroma.

Drug design, anti-tumor activity, and pharmacokinetic study of the anti-fibrin immunoconjugate. Another special feature of our design is the conjugation of highly cytotoxic SN-38 with each mAb, using a specially produced linker composed mainly of PEG, which provided both increased payload capacity and efficient, sustained drug release within the tumor. The branched composition had one maleimide for the attachment of the mAb, one PEG_{12} spacer, and three PEG_{27} ester bonds for the attachment of three SN-38 molecules (Fig. 2A). There were approximately eight thiol residues able to react with the maleimide in the reduced mAb. The calculated drug (SN-38)/mAb ratio of the immunoconjugate was approximately 24. Previous studies have reported drug/mAb ratios in the range 3–8.[26–28] Therefore, the ratio of 24 obtained in the present study is so far the highest, which means that the drug can be carried with the minimum amount of antibody, resulting in a reduction of both undesirable drug effects in the body and production costs.

The conjugated SN-38 had no cytotoxic effect, which means that the cytotoxic immunoconjugate itself is a prodrug. Consequently, we succeeded in producing a cytotoxic immunoconjugate, namely AFCA-branched-PEG-(SN-38)₃, hereafter abbreviated to AFCA-B-P-(SN-38)₃ (Fig. 2A). The immunoconjugate, via the ester bond, was stable in 5% glucose (pH 4.6) because the phenyl ester bond is stable under acidic conditions

and labile under mild alkaline conditions.[29] Under physiological conditions (PBS pH 7.4 and serum) such as in the extracellular environment, the immunoconjugate, via the ester bond, can release SN-38 enzyme independently, gradually, and effectively (Fig. 2B). This bond has already been introduced into clinical use, such as in NK012.[30] The antitumor activity of AFCA-B-P-(SN-38)₃ was evaluated in vivo and, following its administration four times weekly at an equivalent SN-38 dose of 13.3 mg/kg per day, showed significant antitumor activity compared with findings in mice treated with either saline or CPT-11 (40 mg/kg per day at the maximum tolerated dose [MTD], equivalent to a dose of 23.2 mg/kg per day SN-38). Although tumors continued to increase in mice treated with CPT-11, the growth of tumors in mice treated with AFCA-B-P-(SN-38)₃ was significantly suppressed for more than 1 month (Fig. 2C). Thus, AFCA-B-P-(SN-38)₃ exerted strong antitumor activity compared with CPT-11 (Fig. 2C). Although treatment-related body weight loss was observed in mice treated with each of the drugs, there was no significant difference in body weight loss between the control group and the CPT-11- and AFCA-B-P-(SN-38)₃-treated groups (Fig. 2D). Blood tests revealed no significant bone marrow toxicity or liver and kidney dysfunction in any of the treatment groups (data not shown).

Release of SN-38 from the anti-fibrin immunoconjugate induces damage to both tumor cells and tumor vessels. After injection of AFCA-B-P-(SN-38)₃, the concentration of total SN-38 (antibody-bound and unbound forms) and free SN-38 (unbound form) in plasma declined gradually within a week, whereas CPT-11 exhibited rapid clearance (Fig. 3A). We then examined the intratumoral distribution of SN-38 released from the immunoconjugate using HPLC. Significantly high concentrations of total and free SN-38 were detected in tumor tissues treated with the immunoconjugate for 168 hours compared with CPT-11 (Fig. 3B). The second significant observation following
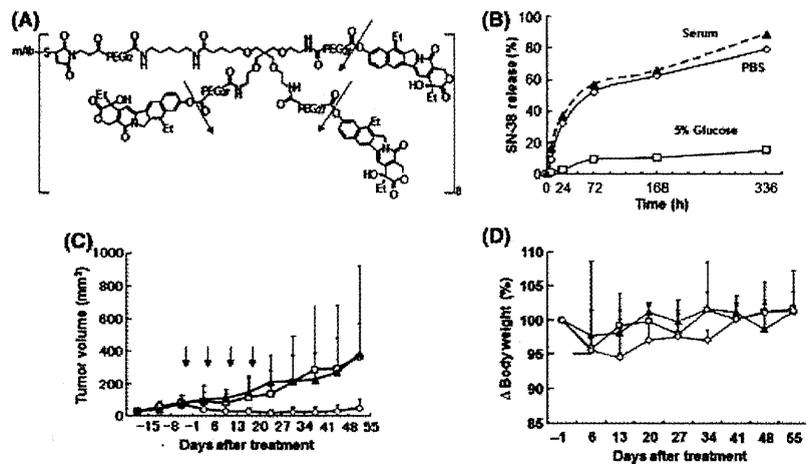
Fig. 2. Drug design, anti-tumor effect and pharmacokinetics of the anti-fibrin immunoconjugate. (A) Drug design of the immunoconjugate: mAb–PEG–three-branched PEG–(SN-38)$_3$ linked via an ester bond. One antibody bears 24 molecules of SN-38. The arrows indicate the cleavage sites to release free active SN-38. (B) Release of SN-38 from immunoconjugates over time in mouse serum, PBS (pH 7.4), or 5% glucose at 37°C. Data show single values determined at each time point. (C) Antitumor activity was examined in vivo. Immunoconjugates (◇), camptothecin-11 (CPT-11; □), or saline (▲), were administered to mice bearing chemical-induced cutaneous tumors via intravenous injection on Days 0, 7, 14, and 21. Arrows indicate the day of administration and the curves illustrate the effect of treatment on tumor size. Data are the mean ± SD ($n = 5$ in each group). $P = 0.0005$ for CPT-11 compared with immunoconjugate; $P < 0.0001$ for saline compared with immunoconjugate. (D) Changes in the relative body weight of mice injected with Immunoconjugates (◇), CPT-11 (□), or saline (▲) on Days 0, 7, 14, and 21. Data are the mean ± SD. There were no significant differences between the three groups ($P = 0.09$ for CPT-11 versus immunoconjugate; $P = 0.0866$ for saline versus immunoconjugate).
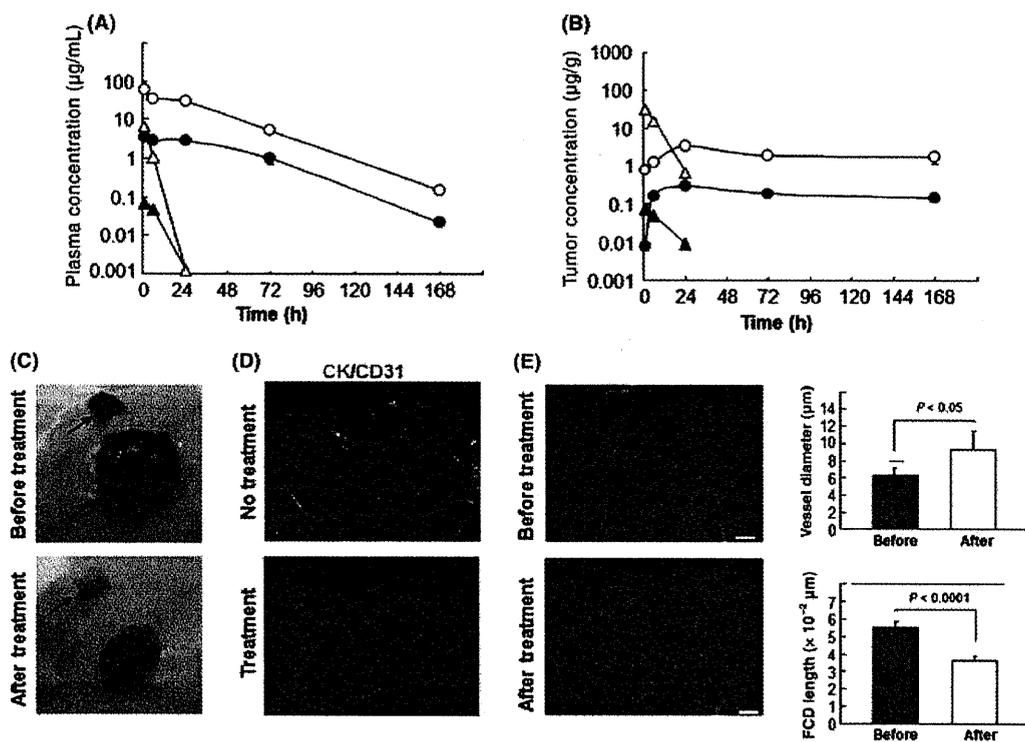
Fig. 3. Drug distribution and antivascular activity of the immunoconjugate. (A,B) Plasma (A) and tumor (B) concentrations of total SN-38 (bound and unbound form; ○), camptothecin-11 (CPT-11; △), and free SN-38 (unbound form) released from the immunoconjugate (●) or converted from CPT-11 (▲) were determined by HPLC 1, 6, 24, 72, and 168 h after injection. (C) The color of the tumor changed from reddish to white 5 days after injection of the immunoconjugate, but not CPT-11. The arrows indicate the position of each tumor. (D) Tumor vessels after injection of the immunoconjugate (Treatment) were examined using CD31 (red) and cytokeratin (CK; green). Untreated mice (No treatment) were used as a control. Scale bar, 100 μm. (E) The left-hand figures show the change of tumor vessels visualized with FITC-dextran before and after the injection of the immunoconjugate, visualized using FITC–dextran by in vivo fiber confocal fluorescence microscopy. Quantified vessel diameter and functional capillary density (FCD) length are shown on the right. Scale bars, 20 μm.

treatment with AFCA-B-P-(SN-38)$_3$ was a change in gross tumor color from reddish to white (Fig. 3C). To clarify the cause for this change in color, the histopathological features of the tumor stroma after immunoconjugate therapy were examined. There was no clear change in fibroblasts or macrophages, which play an important role in tumor progression[31,32] (data not shown). We then evaluated stromal vascular changes both qualitatively and quantitatively using immunohistochemistry and *in vivo* fluorescence endomicroscopy. Using these techniques, discontinuation and irregularity comprising a mixture of narrowness and enlargement of tumor vessels were manifested following treatment with AFCA-B-P-(SN-38)$_3$ (Fig. 3D,E).

Discussion

It is known that LMW ACA, including molecular targeting agents, can easily extravasate from normal blood vessels, resulting in various adverse effects (Fig. 4A). To overcome the off-target effects caused by LMW ACA, an immunoconjugate therapy was developed in which ACA or a toxin is conjugated to a cancer cell-specific mAb (Fig. 4B).

The immunoconjugates selectively extravagate from leaky tumor vessels and this is an advantage in cancer treatment. However, to date, immunoconjugate therapies for common solid tumors have not been successful in clinical practice because of the heterogeneity of the target antigens.[1-6,8,9] Moreover, most human tumors have abundant stroma that hinders the distribution of the immunoconjugate. Our basic strategy for overcoming the stromal barrier as a protective shield for cancer cells is to make use of the fibrin in the stroma as a scaffold assembly of the immunoconjugates, followed by the release of SN-38 to the cancer cells. This free SN-38 can easily reach the cancer cells by diffusion through the stromal barrier. Another important finding of the present study is that SN-38 released from the immunoconjugates and located in the fibrin networks around the tumor vasculature may attack vascular endothelial cells.

During the process of blood coagulation, extrinsically activated thrombin cleaves fibrinopeptides A and B from the α- and β-chains of fibrinogens, generating soluble fibrin monomers. Thereafter, an insoluble fibrin clot forms following enzymatic and non-enzymatic processing.[33] Therefore, it is speculated that the epitope of our anti-fibrin mAb is adjacent to the thrombin cutting site of the fibrinogens.

Another feature of our anti-fibrin mAb is the conversion of human chimeric IgG from mouse IgM using an antibody engineering technique. The use of human chimeras is beneficial for clinical applications to avoid human anti-mouse neutralizing antibodies and allergic reactions in humans. In addition, because of the rapid blood clearance and low penetration of IgM compared with IgG, based on the faster elimination of IgM from the liver and its larger molecular size,[34] IgM is not suitable as a drug delivery vehicle.

The anti-fibrin mAb was conjugated with SN-38 using newly designed linker assembly. SN-38 is a topoisomerase I inhibitor, with time-dependent antitumor activity, and is an active component of CPT-11, which is used clinically in the treatment of
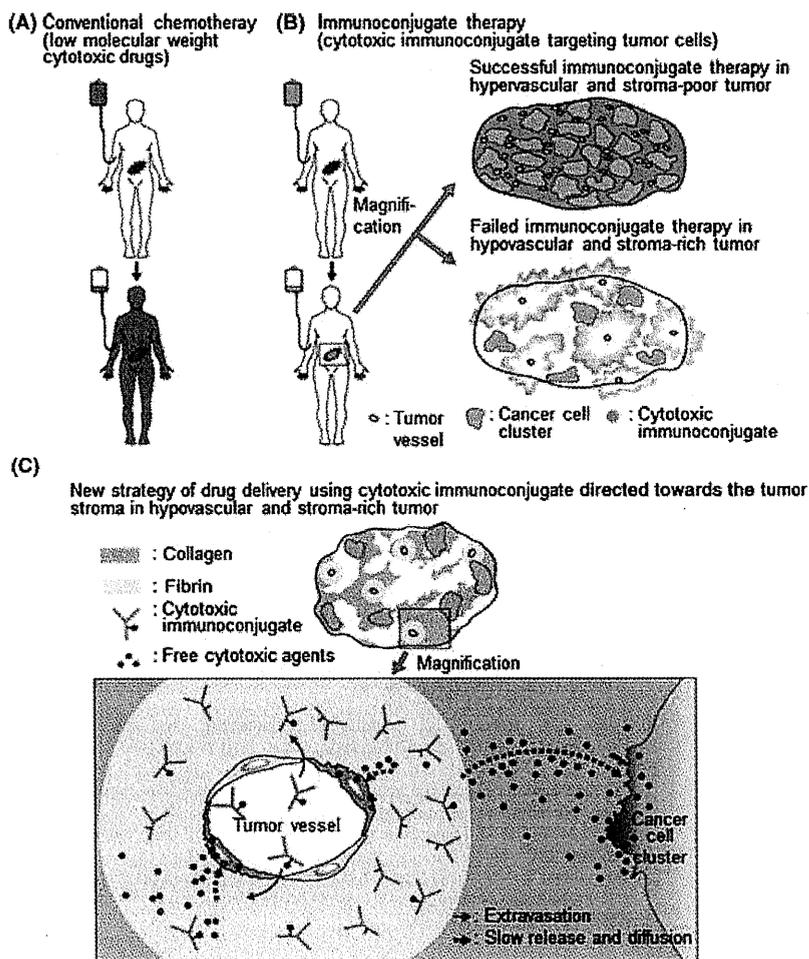

Fig. 4. Diagram of the background and the new concept of drug delivery using tumor stroma as a ligand. (A) Low molecular weight anticancer agents (black) can be distributed throughout the entire body, resulting in serious side effects. (B) Cytotoxic immunoconjugates (blue) accumulate selectively in the tumor tissue. Successful (upper) and failed (lower) immunoconjugate therapy is shown. (C) The newly developed immunoconjugate (i.e. anti-fibrin chimeric IgG–branched-PEG-(SN-38)$_3$) extravasates selectively from leaky tumor vessels, binds specifically to the fibrin network around the tumor vessels to create a scaffold, and then allows the effective, sustained release of SN-38, an anticancer agent with time-dependent effects, from the scaffold. Because this released anticancer agent is of a low molecular weight, it is subsequently distributed throughout the entire tumor stroma, which normally acts as a barrier, and induces damage not only to tumor cells, but also to tumor vessels.

colorectal, lung, and other cancers.[35] Linker technology is an important part of immunoconjugate chemotherapy, and various linkers have been exploited to date. Of these, acid labile hydrazone linkage, thiol reduction of disulfide linkers, and enzymatic proteolysis of peptide linkers have been used successfully to ensure stability in plasma.[26–28] For these types of linkers, cell-mediated endocytosis and intracellular processing of the immunoconjugates are indispensable to make the active agent work. In our newly deployed linker construct, an ester bond can release SN-38 gradually, independent of enzymes, under physiological conditions such as in the extracellular environment. In our design, PEG was combined close to this ester bond. It is known that PEG evades non-specific capture by the reticuloendothelial system (RES) in the body, with the steric structure around the bond protecting against immunoconjugate degradation in the blood. Furthermore, PEG has already been used for this purpose.[11,12] Moreover, the unique branched composition enables the attachment of three SN-38 molecules, rather than only one as in standard linear types of linkers.

As mentioned above, asymptomatic fibrin formation occurs only during cancer invasion and metastasis. Patients with advanced cancer are candidates for treatment with systemic ACA and almost all such patients are fibrin free, except for in the cancer tissue in the body. In addition, HMW proteins, including IgG, cannot extravasate from normal blood vessels to cause unwanted side effects in non-neoplastic organs (Fig. 4C). In spontaneous mouse tumors characterized by abundant stroma, this cancer stroma-targeting therapy using tumor-induced fibrin clots has succeeded, for the first time, in producing conditions that achieve drug exposure levels specifically in tumor cells that are similar to those in monolayer culture dishes and it is thus a highly effective new strategy for treating solid tumors, especially stroma-rich cancers, which are refractory to conventional therapy. In the 1960s, and ^{131}I-Ab that targeted fibrin was suggested as a potential cancer therapy.[36] However, that Ab was polyclonal and reacted with fibrinogen, which is the physiological precursor of fibrin and abundant in the blood stream. The

polyclonal Ab against fibrin bound to fibrinogen in the blood stream and easily changed to a circulating immune complex. This immune complex was eliminated more rapidly from the liver than intact IgG, resulting in rapid blood clearance.[34,37] In fact, the present study demonstrated that the accumulation of the anti-fibrinogen mAb was weaker and that the anti-fibrinogen mAb was eliminated more rapidly than the anti-fibrin chimeric mAb.

This linker technology can be applied to many other ACA, including molecular targeting agents. Thus, this present discovery, the development of which was based on cancer pathophysiology and organic chemistry, may change current therapy with ACA and open a new fields of medical science, consequently producing many useful treatment modalities in the field of oncology, cardiovascular disease, and inflammation.

Disclosure Statement

The authors have no conflict of interest to declare.

References

1 Heng HH, Bremer SW, Stevens JB et al. Genetic and epigenetic heterogeneity in cancer: a genome-centric perspective. J Cell Physiol 2009; 220: 538–47.
2 Hayden E. Cancer complexity slows quest for cure. Nature 2006; 455: 148.
3 Grizzi F, DiIeva A, Russo C et al. Cancer initiation and progression: an unsimplifiable complexity. Theor Biol Med Model 2006; 3: 37.
4 Koenders PG, Peters WH, Wobbes T et al. Epidermal growth factor receptor levels are lower in carcinomatous than in normal colorectal tissue. Br J Cancer 1992; 65: 189–92.
5 Messersmith W, Oppenheimer D, Peralba J et al. Assessment of epidermal growth factor receptor (EGFR) signaling in paired colorectal cancer and normal colon tissue samples using computer-aided immunohistochemical analysis. Cancer Biol Ther 2005; 4: 1381–6.
6 Keshava Prasad TS, Goel R, Kandasamy K et al. Human protein reference database: 2009 update. Nucleic Acids Res 2009; 37: D767–72.
7 Berthiaume JM, Wallace KB. Adriamycin-induced oxidative mitochondrial cardiotoxicity. Cell Biol Toxicol 2007; 23: 15–25.
8 Imai K, Takaoka A. Comparing antibody and small-molecule therapies for cancer. Nat Rev Cancer 2006; 6: 714–27.
9 Ricart AD, Tolcher AW. Technology insight: cytotoxic drug immunoconjugates for cancer therapy. Nat Clin Pract Oncol 2007; 4: 245–55.
10 Matsumura Y, Maeda H. A new concept for macromolecular therapeutics in cancer chemotherapy: mechanism of tumoritropic accumulation of proteins and the antitumor agent smancs. Cancer Res 1986; 46: 6387–92.
11 Matsumura Y. Poly (amino acid) micelle nanocarriers in preclinical and clinical studies. Adv Drug Deliv Rev 2008; 22: 899–914.
12 Duncan R. Polymer conjugates as anticancer nanomedicines. Nat Rev Cancer 2006; 6: 688–701.
13 Dvorak HF. Tumors: wounds that do not heal. Similarities between tumor stroma generation and wound healing. N Engl J Med 1986; 315: 1650–9.

14 Ghajar CM, Bissell MJ. Extracellular matrix control of mammary gland morphogenesis and tumorigenesis: insights from imaging. Histochem Cell Biol 2008; 130: 1105–18.
15 Minchinton AI, Tannock IF. Drug penetration in solid tumors. Nat Rev Cancer 2006; 6: 583–92.
16 Trédan O, Galmarini CM, Patel K, Tannock IF. Drug resistance and the solid tumor microenvironment. J Natl Cancer Inst 2007; 99: 1441–54.
17 Varki A. Trousseau's syndrome: multiple definitions and multiple mechanisms. Blood 2007; 110: 1723–9.
18 Shoji M, Hancock WW, Abe K, Micko C. Activation of coagulation and angiogenesis in cancer: immunohistochemical localization in situ of clotting proteins and vascular endothelial growth factor in human cancer. Am J Pathol 1998; 152: 399–411.
19 Stein PD, Beemath A, Meyers FA, Skaf E. Incidence of venous thromboembolism in patients hospitalized with cancer. Am J Med 2006; 119: 60–8.
20 Belting M, Ahamed J, Ruf W. Signaling of the tissue factor coagulation pathway in angiogenesis and cancer. Arterioscler Thromb Vasc Biol 2005; 25: 1545–50.
21 Hirakawa S, Kodama S, Kunstfeld R et al. VEGF-A induces tumor and sentinel lymph node lymphangiogenesis and promotes lymphatic metastasis. J Exp Med 2005; 201: 1089–99.
22 Filler RB, Roberts SJ, Girardi M. Cutaneous two-stage chemical carcinogenesis. CSH Protoc 2007; 2007: doi:10.1101/pdb.prot4837.
23 Lin KY, Maricevich M, Bardeesy N et al. In vivo quantitative microvasculature phenotype imaging of healthy and malignant tissues using a fiber-optic confocal laser microprobe. Transl Oncol 2008; 1: 84–94.
24 Ellis LM, Fidler IJ. Finding the tumor copycat. Therapy fails, patients don't. Nat Med 2010; 16: 974–5.
25 Hawighorst T, Velasco P, Streit M et al. Thrombospondin-2 plays a protective role in multistep carcinogenesis: a novel host anti-tumor defense mechanism. EMBO J 2001; 20: 2631–40.

26 Doronina SO, Toki BE, Torgov MY *et al.* Development of potent monoclonal antibody auristatin conjugates for cancer therapy. *Nat Biotechnol* 2003; **21**: 778–84.
27 Wu AM, Senter PD. Arming antibodies: prospects and challenges for immunoconjugates. *Nat Biotechnol* 2005; **23**: 1137–46.
28 Lewis Phillips GD, Li G, Dugger DL *et al.* Targeting HER2-positive breast cancer with trastuzumab-DM1, an antibody-cytotoxic drug conjugate. *Cancer Res* 2008; **68**: 9280–90.
29 Koizumi F, Kitagawa M, Negishi T *et al.* Novel SN-38-incorporating polymeric micelles, NK012, eradicate vascular endothelial growth factor-secreting bulky tumors. *Cancer Res* 2006; **66**: 10.
30 Hamaguchi T, Doi T, Eguchi-Nakajima T *et al.* Phase I study of NK012, a novel SN-38-incorporating micellar nanoparticle, in adult patients with solid tumors. *Clin Cancer Res* 2010; **16**: 5058–66.
31 Bhowmick NA, Neilson EG, Moses HL. Stromal fibroblast in cancer initiation and progression. *Nature* 2004; **432**: 332–7.
32 Alderton GK. Tumor microenvironment: macrophages lead the way. *Nat Rev Cancer* 2010; **10**: 162–3.
33 Mosesson MW. Fibrinogen and fibrin structure and functions. *J Thromb Haemost* 2005; **3**: 1894–904.
34 Rehlaender BN, Cho MJ. Antibodies as carrier proteins. *Pharm Res* 1998; **15**: 1652–6.
35 Pommier Y. Topoisomerase I inhibitors: camptothecins and beyond. *Nat Rev Cancer* 2006; **6**: 789–802.
36 Bale WF, Spar IL, Goodland RL. Experimental radiation therapy of tumors with I^{131}-carrying antibodies to fibrin. *Cancer Res* 1960; **20**: 1488–94.
37 Finbloom DS, Magilavy DB, Harford JB, Rifai A, Plotz PH. Influence of antigen on immune complex behavior in mice. *J Clin Invest* 1981; **68**: 214–24.

Supporting Information

Additional Supporting Information may be found in the online version of this article:

Data S1. Detailed information regarding the synthesis of branched linker, branched PEG-linked SN-38, and NMR spectra for each compound.

Please note: Wiley-Blackwell are not responsible for the content or functionality of any supporting materials supplied by the authors. Any queries (other than missing material) should be directed to the corresponding author for the article.

Cancer-Stroma Targeting Therapy by Cytotoxic Immunoconjugate Bound to the Collagen 4 Network in the Tumor Tissue

Masahiro Yasunaga,[†] Shino Manabe,[‡] David Tarin,[§] and Yasuhiro Matsumura[*,†]

[†]Investigative Treatment Division, Research Center for Innovative Oncology, National Cancer Center Hospital East, 6-5-1 Kashiwanoha, Kashiwa, Chiba, 277-8577, Japan

[‡]Synthetic Cellular Chemistry Laboratory, RIKEN Advanced Science Institute, 2-1 Hirosawa, Wako, Saitama 351-0198, Japan

[§]Department of Pathology and Moores/UCSD Comprehensive Cancer Center, University of California, San Diego, 3855 Health Sciences Drive MC 0803, La Jolla, California, 92093-0803, United States

ABSTRACT: Some cytotoxic immunoconjugates have been approved for malignant lymphoma, a representative of hypervascular and stroma-poor tumors. However, many human solid tumors possess abundant intercellular stromata that prevent diffusion of cancer cell-specific monoclonal antibodies (mAb) and become a barrier preventing immunoconjugates from directly attacking cancer cells. Here we show the successful development of a new strategy that overcomes this drawback and achieves a highly localized concentration of a topoisomerase I inhibitor, SN 38, by conjugating it via an ester bond to a mAb targeted against collagen 4, a plentiful component of the tumor stroma. Poly(ethylene glycol) (PEG) was utilized as a spacer, close to each bond, to maintain stability in the blood. Immunoconjugates selectively extravasated from leaky tumor

vessels and minimally from normal vessels because the immunoconjugates are too large to pass through normal vessel walls. Stroma-targeting immunoconjugates bound to the stroma to create a scaffold, from which sustained release of cytotoxic agent occurred and the agent subsequently diffused throughout the tumor tissue to damage both tumor cells and vessels. Cancer-stroma-targeting immunoconjugate therapy was thus validated as a new modality of oncological therapy, especially for refractory, stromal-rich cancers.
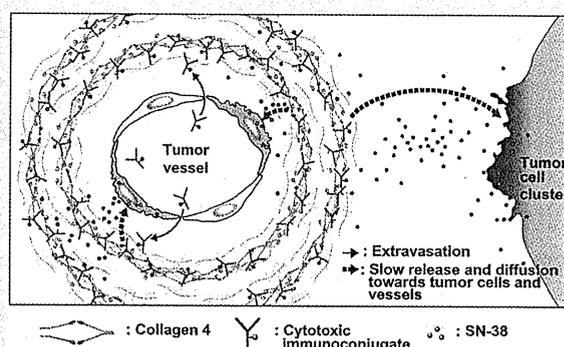
■ INTRODUCTION

In contrast to low molecular weight (LMW) agents, high molecular weight (HMW) agents such as monoclonal antibodies (mAbs) and nanoparticles have a long plasma half-life because they are too large to pass through the normal vessel walls, unless they are trapped by the reticuloendothelial system (RES) in various organs. However, HMW agents can reach tumor tissue sufficiently and extravasate efficiently from leaky tumor vessels to achieve tumor-selective accumulation of HMW agents by utilizing the enhanced permeability and retention (EPR) effect.[1-6] Even so, the use of HMW agents presents a dilemma for cancer therapy because the very properties that favor their high accumulation in the lesion also cause low diffusion of these macromolecules within a tumor.[7] Most human solid tumors possess abundant stromata that prevent mAb diffusion and, consequently, become a barrier preventing mAb from directly attacking cancer cells.[7-10] In fact, immunoconjugate therapies for common solid tumors (e.g., colorectal, lung, and pancreatic cancers) have not yet proven successful in clinical practice because of the heterogeneity of target antigens and the low uptake and retention of chemotherapeutic drugs in these types of cancer. This contrasts with the results seen in treatment of human hematologic malignancies and of tumor xenografts in mice, which usually have less inert interstitial tissue within the

neoplasm.[11] The kinetics of drug distribution within tumors are considered to be functions of interstitial conductivity, which is determined by the quantity and density of the extracellular matrix (ECM e.g., proteoglycan, fibronectin), and fibrosis (e.g., collagen fibers) in the stroma.[7-10] Such compact assemblies of various tissue constituents in solid tumors cause reduced drug penetration and also act as a stromal barrier to prevent the diffusion of mAbs (HMW proteins).[7-9,11-13] Although there are a few papers describing tumor stromal targeting using immunoconjugates, the target molecule was still a surface antigen on cells in tumor stroma, or the ECM was used for targeting the tumor vascular endothelial cell.[14,15] The principle of our strategy is that our newly developed immunoconjugates selectively extravasated from leaky tumor vessels, bound to the collagen network in the stroma, and created a scaffold from which effective sustained release of the time-dependent ACA SN-38 occurred. This free SN-38 can easily reach the cancer cells by diffusion through the stromal barrier. Another important finding is that SN-38 released from immunoconjugates can attack and destroy the vascular endothelial cells (Figure1).

Conventional cell targeting immunoconjugate therapy

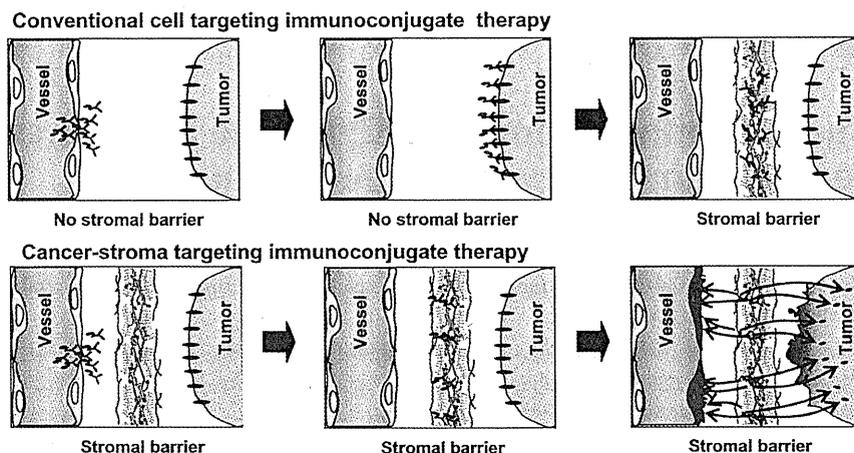**Cancer-stroma targeting immunoconjugate therapy**

Figure 1. Therapeutic strategy of cancer-stroma targeting immunoconjugate. Conventional immunoconjugates can target cancer cells in the treatment of stroma-poor cancer such as malignant lymphoma. However, Many human solid tumors possess abundant stromata hindering the distribution of the immunoconjugates against cancer cells themselves (stromal barrier), whereas newly developed cancer-stroma-targeting immunoconjugates bound to the collagen 4 network of the cancer stroma, from which effective sustained release of the time-dependent anticancer agent SN-38 occurred. The SN-38 subsequently diffused throughout the tumor tissue to damage both cancer cells and vessels. Arrows show the distribution of SN-38 beyond the stromal barrier.

■ EXPERIMENTAL PROCEDURES

Antibody/Drug, Reagents, and Cells. Anti-EpCAM antibody-producing hybridoma (B8-4) was established from a mouse with immunizing recombinant protein (R&D Systems, Minneapolis, MN, USA). Anti-collagen 4 antibody-producing hybridoma (35-4) was obtained from a rat by immunization with purified mouse collagen 4 protein. A carrier protein was not used in either case.[16,17] Spleen cells from each immunized animal were fused with myeloma cells (P3X63Ag8.653). The specific hybridoma clones were selected using ELISA. Our anticollagen 4 antibody (35-4) was specific for mouse protein but not for human (data not shown). Antihuman CD20 antibody (rituximab) was purchased from Daiichi-Sankyo (Tokyo, Japan). For immunohistochemistry, polyclonal anti-collagen 4 antibody (LSL-LB-1403), monoclonal anti-CD31 antibody (MEC 13.3) and polyclonal anti-CD31 antibody (AF3628) were purchased from Cosmo. Bio. Inc. (Tokyo, Japan), Becton, Dickinson and Company (Franklin Lakes, NJ, USA), and R&D Systems, Inc. (Minneapolis, MN USA), respectively. SN-38 and CPT-11 (irinotecan) were purchased from Tokyo Chemical Industry Co. (Tokyo, Japan) and Yakult (Tokyo, Japan), respectively. Human pancreatic cancer cell line, PSN1 was purchased from the American Type Culture Collection (Rockville, MD, USA). Human pancreatic cancer cell line SUIT2 was purchased from the Health Science Research Resources Bank (Osaka, Japan). PSN1 and SUIT2 were maintained in DMEM (Sigma) supplemented with 10% fetal bovine serum (Tissue Culture Biologicals, CA, USA), penicillin, streptomycin, and amphotericin B (Sigma) in an atmosphere of 5% CO_2 at 37 °C. RL was maintained in RPMI1690 (Sigma) instead of DMEM.

Antibody Conjugate. A linker containing an ester bond between PEG and SN-38 was produced as follows. To a solution of SN-38 (102.1 mg, 0.260 mmol), BocHN-PEG$_{27}$-COOH (407.1 mg, 0.286 mmol) and 4-dimethylamino pyridine (15.9 mg, 0.130 mmol) in DMF (1 mL), 1-ethyl-3-(3-dimethyl aminopropyl)-carbodiimide·HCl (54.8 mg, 0.286 mmol) was added at 0 °C. The mixture was stirred at room temperature for

19 h, and the reaction mixture was purified by gel filtration column chromatography (LH20 CHCl$_3$/MeOH 1:1) and then silica gel column chromatography (CHCl$_3$/MeOH 15:1—9:1) to give the ester (420.1 mg, 90%) as a colorless oil.

^{1}H NMR (CD$_3$OD) δ 8.20 (d, J = 9.2 Hz, 1H), 7.99 (s, 1H), 7.66 (m, 2H), 5.60 (d, J = 16.5 Hz, 1H), 5.40 (d, J = 16.5 Hz, 1H), 5.32 (m, 2H), 3.93 (t, J = 6.4 Hz, 2H), 2.96 (t, J = 6.4 Hz, 2H), 1.97 (m, 2H), 1.43 (s, 9H), 1.40 (t, J = 7.6 Hz, 3H), 1,02 (t, J = 7.8 Hz, 3H); ^{13}C NMR (DMSO-d$_6$) δ 164.8, 161.9, 149.2, 148.5, 143.1, 142.7, 141.3, 138.2, 137.7, 137.5, 122.4, 119.5, 118.9, 117.2, 110.7, 106.5, 89.7, 70.4, 64.6, 62.3, 62.0, 62.0, 62.0, 61.9, 61.8, 61.8, 61.7, 61.5, 58.1, 58.0, 57.1, 41.2, 40.1, 31.8, 28.1, 26.3, 19.4, 14.4, 4.9, −1.1.

To a solution of BocHN-PEG$_{27}$-SN-38 (221.5 mg, 0.123 mmol) in CH$_2$Cl$_2$ (10 mL), trifluoroacetic acid (1 mL) was added at room temperature. After the mixture was stirred for 1.5 h, the solvent was removed in vacuo, and toluene was added. After evaporation, the residue was dried under high vacuum. The residue was dissolved in CH$_2$Cl$_2$ (5 mL) and MAL-PEG$_{12}$-NHS (128.2 mg, 0.148 mmol) and iPr$_2$NEt (48 μL, 0.246 mmol) were added at 0 °C. After 30 min, the mixture was purified by gel filtration column chromatography (LH-20, CHCl$_3$/CH$_3$OH = 1:1) and silica gel column chromatography to give (276.0 mg, 91%) of the target product as a colorless oil.

^{1}H NMR (CD$_3$OD) δ 8.20 (d, J = 9.2 Hz, 1H), 8.00 (s, 1H), 7.66—7.64 (m, 2H), 6.83 (s, 2H), 5.60 (d, J = 16.0 Hz, 1H), 5.41 (d, J = 16.0 Hz, 1H), 5.34 (s, 1H), 3.93 (t, J = 6.0 Hz, 2H), 2.97 (t, J = 6.0 Hz, 2H), 2.49—2.45 (m, 4H), 2.00—1.98 (m, 2H), 1.41 (t, J = 7.6 Hz, 3H), 1.02 (t, J = 7.6 Hz, 3H); ^{13}C NMR (DMSO-d$_6$) δ 172.1, 170.4, 169.8, 169.7, 169.1, 156.5, 151.7, 149.7, 148.9, 146.2, 145.6, 145.0, 134.3, 131.1, 128.4, 126.8, 125.3, 118.8, 115.0, 96.5, 72.3, 69.9, 69.6, 69.5, 69.4, 69.0, 68.9, 66.7, 65.8, 65.1, 49.5, 36.0, 34.8, 34.1, 33.9, 31.6, 30.3, 25.4, 22.3, 13.9, 7.8.

Interchain disulfides of the antibodies were first reduced with 10 mM DTT (Sigma).[18] The numbers of free thiols were quantified with dinitrothiocyanobenzene (DNTB, Wako). After the purification by gel filtration (Amicon Ultra Centrifugal Filter Devices, Millipore, Billerica, MA, USA), reduced antibodies
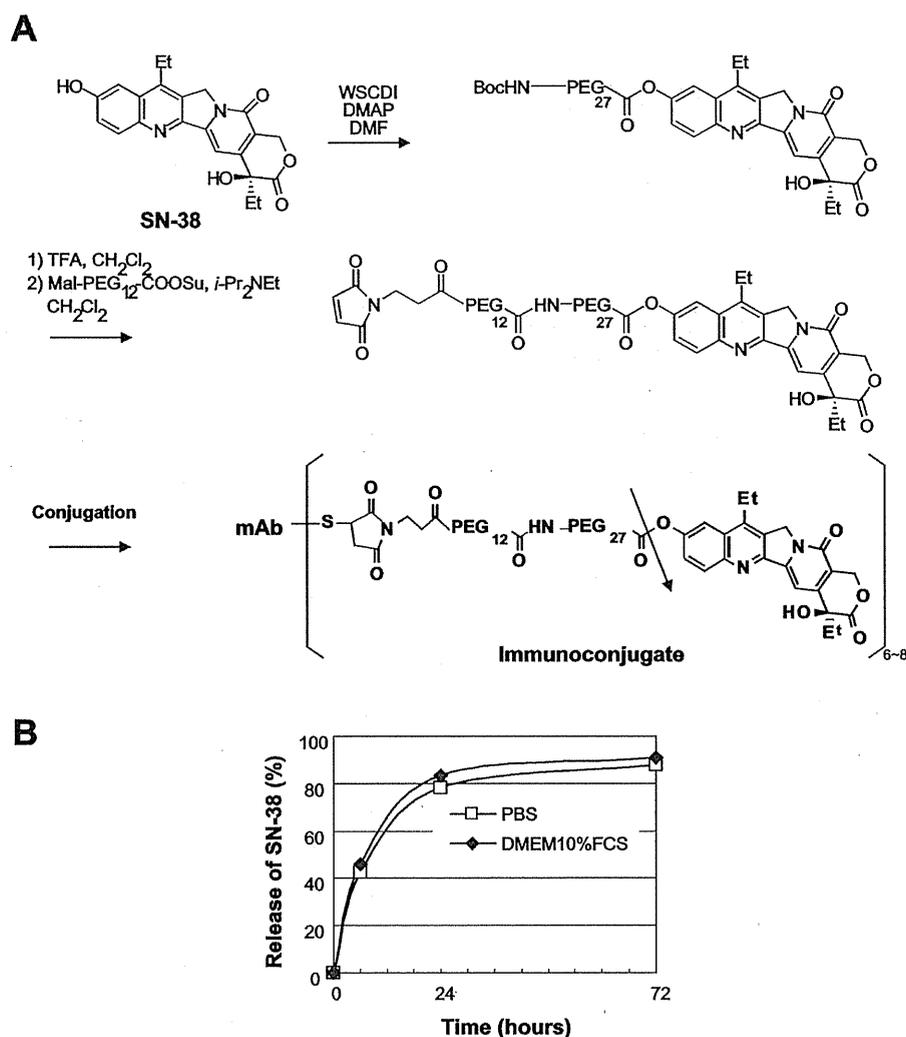
Figure 2. Structure and drug-release of the immunoconjugate. (A) Synthetic scheme of the immunoconjugate. The arrow indicates the cleavage site for releasing free active SN-38. PEG = poly(ethylene glycol). (B) The release behavior (nonenzymatic hydrolysis) of SN-38 from the immunoconjugates.

(3.3 μM) were reacted with the SN-38 prodrugs (13.2 × [number of free thiols] μM) in PBS containing 5 mM EDTA (pH 6) at room temperature for 1 h, then at 4 °C overnight. SN-38-conjugated antibodies were purified by gel filtration (Amicon Ultra Centrifugal Filter Devices, Millipore). The concentration of antibody—prodrug conjugates was determined using the Bradford method (Bio-Rad Protein Assay, 500-0006JA, Bio-Rad). The numbers of residual thiols were quantified with DNTP. Each drug (SN-38)/antibody ratio was determined by comparison between the numbers of free and residual thiols (range from 6.7 to 8.4, Figure 2). For the evaluation of the antibody—drug coupling, the amount of forcibly detached SN-38 from the immunoconjugate was evaluated using HPLC (see next section).

High-Performance Liquid Chromatography (HPLC). The release behavior (nonenzymatic hydrolysis) of SN-38 from the immunoconjugates was investigated in vitro at 37 °C in DMEM with 10% FCS or PBS (pH 7.4). In addition to these reaction solutions at 6, 24, and 72 h in vitro, plasma and tumors on days 1, 3, and 7 after immunoconjugate injection in animal models were obtained. Reaction solutions and plasma were mixed with 0.1 M

HCl at 50% (w/w). Tumors were rinsed with physiological saline, mixed with 0.1 M glycine-HCl buffer (pH 3.0) in methanol at 5% (w/w), and homogenized. To detect free SN-38 in the plasma, samples (50 μL) were mixed with 20 μL of 1 mM phosphoric acid in methanol (1:1) and 100 μL of camptothecin as internal standard solution. To detect free SN-38 in the tumor, samples (100 μL) were mixed with 20 μL of 1 mM phosphoric acid in methanol (1:1), 40 μL of ultrapure water, and 60 μL of internal standard solution. The samples were vortexed vigorously for 10 s and filtered through Ultrafree-MC centrifugal filter devices (Millipore, Bedford, MA, USA). To detect bound SN-38 in the immunoconjugate product itself, plasma or tumor samples (20 μL of plasma, 100 μL of tumor) were diluted with 20 μL of methanol (50% [w/w]) and 20 μL of NaOH (0.7 M). The samples were incubated for 15 min at room temperature. After incubation, 20 μL of HCl (0.7 M) and 60 μL of internal standard solution were added to the samples, and then the hydrolysate was filtered. Reverse-phase high-performance liquid chromatography (HPLC) was conducted at 35 °C on a Mightysil RP-18 GP column (150 mm × 4.6 mm; Kanto

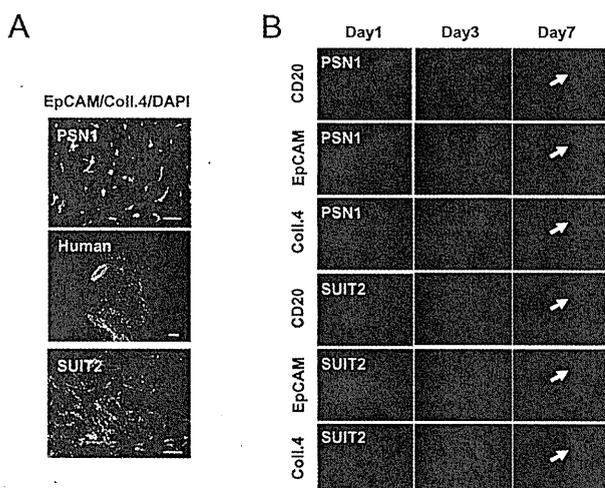## A

EpCAM/Coll.4/DAPI

B

Figure 3. Intratumor accumulation of anti-EpCAM mAb and anti-collagen 4 mAb. (A) PSN1 and SUIT2 tumor and human pancreatic cancer were stained with anti-EpCAM (green), anticollagen 4 (red) mAb, and DAPI (blue). Scale bar = 100 μm. (B) In vivo imaging analysis of PSN1 and SUIT2 tumor was conducted using near-infrared labeled anti-CD20 (control), EpCAM, and collagen (coll.) 4 mAbs on days 1, 3, and 7 after injection. Arrows indicate each tumor position.

Chemical, Tokyo, Japan). The samples were injected into an Alliance Water 2795 HPLC system (Waters, Milford, MA, USA) equipped with a Waters 2475 multi-λ fluorescence detector. The detector was set at 365 and 540 nm (excitation and emission wavelengths, respectively) for SN-38.

In Vivo Imaging and Immunohistochemistry. Antibodies were conjugated with IRDye 800 (Li-Cor Biosciences, Lincoln, NE, USA) according to the manufacturer's protocol and injected to the tail vein at 100 μg. In vivo fluorescence imaging was performed by illuminating the animal using the OV110 small animal imaging system (Olympus Corp., Tokyo, Japan). Human specimens were purchased from US Biomax, Inc. (Rockville, MD, USA) and BioChain Institute, Inc. (Hayward, CA, USA). The tissues were incubated with anti-CD31 antibody (MEC 13.3 or AF3628), anti-collagen 4 antibody (35-4 or LSL-LB-1403), and anti-CD20 (rituximab) or anti-EpCAM antibody (B8-4) as first antibodies and Alexa 488- or 555-labeled anti-human, -mouse, -rat, or -goat IgG (Invitrogen) as second antibodies, respectively.

Animal Model and Antitumor Effects. Female BALB/c nude mice (5 weeks old) were purchased from SLC Japan (Shizuoka, Japan). Mice were inoculated subcutaneously in the flank with 2 × 10⁶ cells of PSM1 and SUIT2. The length (L) and width (W) of tumor masses were measured every 4 days, and tumor volume was calculated using ($L \times W^2$)/2. All animal procedures were performed in compliance with the Guidelines for the Care and Use of Experimental Animals established by the Committee for Animal Experimental of the National Cancer Center. These guidelines meet the ethical standards required by law and also comply with the guidelines for the use of experimental animals in Japan. When the mean tumor volume reached approximately 90 mm³ for PSM1 or approximately 70 mm³ for SUIT2, mice were randomly divided into groups consisting of 5 mice each. Immunoconjugates were administered on day 0 by tail vein injection. The injection doses of antibody—SN-38 prodrug equal

to an SN-38 dose of 3 mg/kg were determined by the calculation based on each drug (SN-38)/antibody ratio.

Statistical Analysis. Data were analyzed using ANOVA (Figure 4A,C) and Student's t test (Figure 4B). $P < 0.05$ was considered as significant.

RESULTS

Preparation of Cytotoxic Immunoconjugates. We developed two mAbs for tumor targeting, one against mouse collagen 4 abundantly found in the stroma of solid tumors, and another against human EpCAM which is strongly expressed in human cancer cells (Figure 3A). The third one was the mAb against CD20, which was used as a nonspecific control mAb for the human epithelial cancer cell lines. We used these three mAbs as vehicles to selectively exit the vascular system through the leaky tumor vessels and distribute within each tumor according to the nature of tumor stroma. Another special feature of our design was to conjugate highly cytotoxic SN-38 with each mAb using a specially selected linker, which provided both high serum stability and efficient, sustained drug release within the tumor lesion. SN-38 is a topoisomerase 1 inhibitor and an active component of CPT-11, which is used clinically for colorectal, lung, and other cancers. For the mAb conjugation to phenol—OH in SN-38, an ester bond was selected. In our design, poly(ethylene glycol) (PEG) was combined close to the bond mentioned above (Figure 2A). PEG is known to evade non-specific capture by RES. The steric structure around the bond protects against immunoconjugate degradation in the blood. PEG has already been used for this purpose. [1-3,5,6] The drug (SN-38)/mAb ratio (the number of drugs attached to a mAb) of each immunoconjugate ranged from 6.7 to 8.4, which was calculated using DNTP method and validated by the evaluation of bound SN-38 in the conjugate using HPLC. Moreover, antigen recognition activity was estimated. In physiological conditions (nonenzymatic hydrolysis), the immunoconjugate can release SN-38 gradually and effectively (Figure 2B).

Intratumor Distribution of Anti-EpCAM mAb and Anti-collagen 4 mAb in Stroma-Poor or -Rich Tumors. We next clarified which types of xenograft tumors generated from human cell lines were stroma-rich or -poor. Immunohistochemistry using our 2 mAbs showed that tumors generated by the PSN1 cell line contained EpCAM-positive cells with interspersed collagen 4-positive stroma, different from that of freshly resected human pancreatic cancer (Figure 3A). On the other hand, SUIT2 tumor, reported as having histopathology relatively resembling the original human pancreatic cancer,[19,20] showed EpCAM-positive cells surrounded by a relatively high amount of collagen 4-positive stroma (Figure 3A). We then investigated the kinetics of entry of mAbs into the tumors using an in vivo imaging system with near-infrared fluorescence, which can provide deep tissue imaging with high fidelity.[21,22] Anti-CD20 mAb (rituximab), which is specific to human B cell lymphoma but not to carcinoma, was used as a nonspecific control because of its high specificity with less background.[11,23] Until day 3, all mAbs labeled with a near-infrared fluorescence dye including the control mAb were delivered to and retained in both PSN1 tumors, and SUIT2 tumors, indicating passive targeting by the EPR effect (Figure 3B). On day 7, anti-CD20 mAb was almost eliminated, but anti-EpCAM and anti-collagen 4 mAb were still retained in both types of tumors, indicating active targeting and retention, that is, binding to their respective ligands within the lesion.